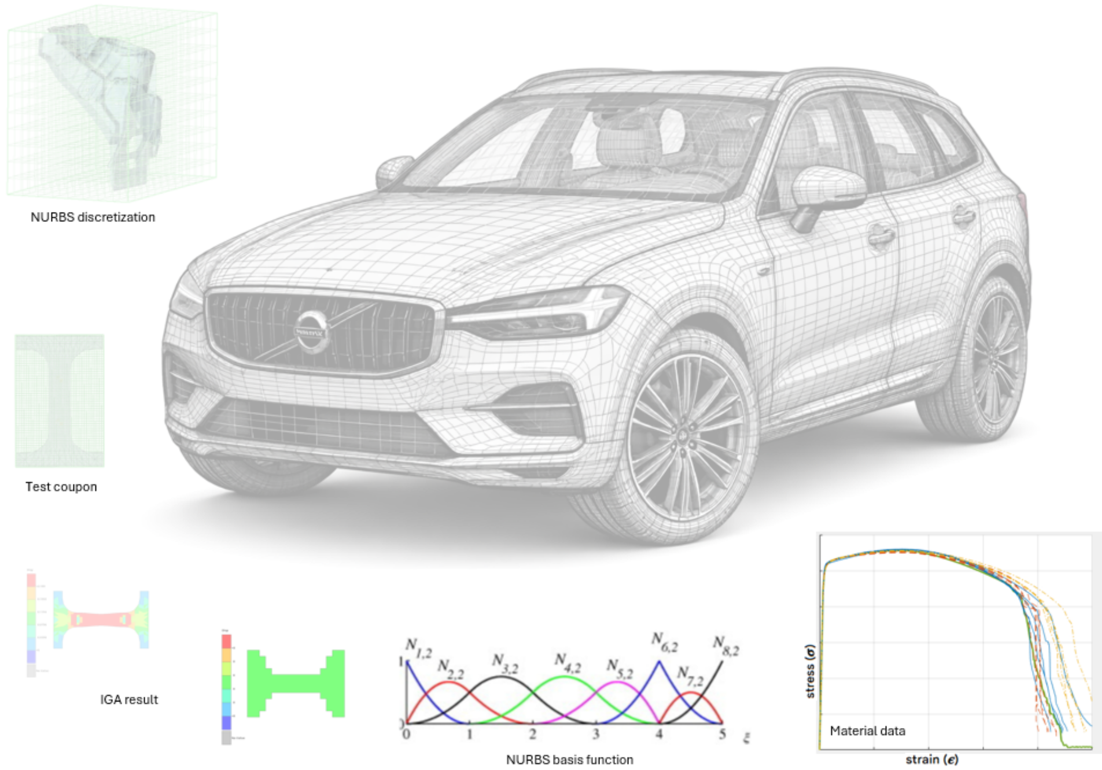

Iso-Geometric Analysis for Crash Simulation: Study of Anisotropy and Fracture Behaviour in Extruded Aluminium Structures

Master's thesis in Materials Engineering

MOHAMMED SHAMIM

DEPARTMENT OF INDUSTRIAL AND MATERIAL SCIENCE

CHALMERS UNIVERSITY OF TECHNOLOGY
Gothenburg, Sweden 2026
www.chalmers.se

Master's thesis 2026

Iso-Geometric Analysis for Crash Simulation: Study of Anisotropy and Fracture Behaviour in Extruded Aluminium Structures

MOHAMMED SHAMIM

Department of Industrial and Material Science
Chalmers University of Technology
Gothenburg, Sweden 2026

Iso-Geometric Analysis for Crash Simulation: Study of Anisotropy and Fracture Behaviour in Extruded Aluminium Structures
MOHAMMED SHAMIM

Supervisor: Per-Anders Eggertsen, Volvo Cars Corporation
Examiner: Johan Ahlström, Department of Mechanical Engineering

Master's Thesis 2026
Department of Industrial and Material Science
Materials Engineering
Chalmers University of Technology
SE-412 96 Gothenburg
Telephone +46 31 772 1000

Cover: Iso-Gemetry NURBS based model for FE analysis.

Typeset in LaTeX
Printed by Chalmers Reproservice
Gothenburg, Sweden 2026

Isogeometric Analysis for Crash Simulation: Study of Anisotropy and Fracture Behaviour in Extruded Aluminium Structures
MOHAMMED SHAMIM
Department of Industrial and Material Science
Chalmers University of Technology

Abstract

Achieving reliable crash and impact simulations is essential for improving vehicle safety, reducing development time, and minimizing costs associated with physical testing. Although the finite element (FE) method remains the established standard for crashworthiness analysis in the automotive industry, its dependence on mesh generation, geometric approximation, and reduced continuity can limit predictive accuracy and efficiency in complex structural applications.

Isogeometric Analysis (IGA) has emerged as a promising alternative by directly incorporating computer-aided design (CAD) geometry into numerical simulation through spline-based basis functions. This framework enables exact geometry representation and higher-order continuity, offering improved capability for capturing nonlinear deformation, stress evolution, and damage initiation under crash-relevant loading conditions.

This study investigates the applicability of IGA to automotive crash simulations, with particular emphasis on the anisotropic behaviour of extruded aluminium components and stress triaxiality-dependent ductile fracture. Numerical investigations are carried out across multiple scales, ranging from material characterisation via tensile testing to component- and assembly-level crash simulations.

The study includes a systematic evaluation of strain formulations, refinement strategies, and solid discretisation approaches, motivated by the need to improve correlation between numerical simulations and physical testing at Volvo Cars.

The results demonstrate that IGA improves geometric fidelity and produces smoother and more stable solution fields, leading to enhanced prediction of stress distribution, deformation patterns, and damage evolution compared to conventional FE formulations. However, challenges remain, including numerical locking phenomena, sensitivity to discretisation parameters, convergence issues in highly nonlinear regimes, and limitations in preprocessing workflows and implementation complexity.

Overall, IGA shows strong potential for high-fidelity crash simulation, although further developments are required to improve robustness and enable efficient large-scale industrial applications.

Keywords: IGA, FEA, NURBS, GISSMO, Triaxiality, Failure strain, Volumetric locking, Solid elements, Anisotropy.

Acknowledgements

I would like to express my sincere gratitude to my supervisor, Per-Anders Eggertsen, for his invaluable guidance, continuous encouragement, and constructive feedback throughout the course of this thesis. His expertise, availability, and commitment have been instrumental in shaping both the direction and the quality of this research.

I am also deeply grateful to Mats Landervik for his insightful suggestions, thoughtful discussions, constructive perspectives, and support with MATLAB-related work, all of which have significantly contributed to enhancing the clarity and academic rigor of this research.

My sincere appreciation goes to Johan Jergeus, Eric Bojestig, and Jonas Hultman at Volvo Cars for their technical support, collaborative engagement, and practical insights. Their willingness to share their expertise, particularly in the field of materials, has been essential to the successful execution of this project.

Additionally, I would like to extend my thanks to all my colleagues at Volvo Cars who have contributed in various ways to this project. Their encouragement and professional input have made this journey both productive and enjoyable.

I would also like to express my sincere appreciation to the LS-DYNA support team for their valuable technical assistance and insightful guidance in addressing solver-related challenges, which significantly improved the robustness and reliability of the simulations.

I would also like to acknowledge Johan Ahlström, my examiner, for his careful evaluation, valuable comments, and commitment to maintaining high academic standards. His feedback has played an important role in refining and finalizing this thesis.

In addition, I am thankful to my fellow students and friends at Chalmers University of Technology for their support, engaging discussions, and collaborative spirit throughout my studies. Their encouragement and camaraderie have contributed to a stimulating and motivating academic environment.

Finally, I would like to express my deepest gratitude to my wife and my son (Hamza), as well as my family, for their unwavering support, patience, and belief in me. Their constant encouragement and understanding have been a vital source of strength throughout this academic journey.

Mohammed Shamim, Gothenburg, June 2026

List of Acronyms

Below is the list of acronyms that have been used throughout this thesis listed in alphabetical order:

CAD	Computer-Aided Design
FEA	Finite Element Analysis
GISSMO	Generalized Incremental Stress State Dependent Damage Model
IGA	Isogeometric Analysis
NURBS	Non-Uniform Rational B-Splines

Contents

List of Figures

List of Tables

1

Introduction

Ensuring reliable crash and impact simulations is essential to improve vehicle safety, shorten development cycles, and reduce dependence on costly physical tests. In the automotive industry, traditional finite element (FE) methods have long served as the principal tool for crashworthiness assessment. However, despite their widespread adoption, conventional FE approaches often involve labor-intensive meshing procedures and require geometry simplifications that may compromise both computational efficiency and predictive accuracy when analyzing complex structures.

As modern vehicles evolve toward lighter, modular and increasingly performance-driven architectures, the demand for simulation techniques capable of accurately predicting crash behaviour across components, sub–assemblies, and full-vehicle systems continues to grow. This requirement is further intensified by the growing use of advanced materials that exhibit anisotropic mechanical properties-behaviour strongly influenced by manufacturing processes such as rolling, forming, casting, or extrusion. Accurately capturing this anisotropy is critical for realistic crash simulations and for the development of safer, more optimised vehicle designs.

In industrial practice, aluminum components are predominantly produced using either extrusion or casting. Although both methods result in distinct material responses, this thesis focuses on extruded aluminum. Extruded aluminum offers outstanding ductility, high strength-to-weight ratios, and the ability to form complex cross-sections that surpass the geometric freedom of steel. The material also often exhibits significant plasticity and fracture anisotropy, and recent technological advancements now enable the fabrication of closed-section profiles with variable wall thicknesses. These improvements further enhance their relevance within automotive engineering, particularly in areas that require lightweight solutions without compromising crash performance. A notable advantage of extruded aluminum is its excellent bendability, which enables efficient energy absorption during impact events. This characteristic reduces load transfer throughout the structure and contributes to improved occupant protection-qualities that make extruded aluminum a compelling material for modern crash-critical applications.

In response to increasing structural and material complexity, Volvo Cars Corporation is investigating Iso-Geometric Analysis (IGA) as a potential alternative to traditional

FE methods for crash simulation. IGA offers a unified representation of geometry and analysis, potentially reducing meshing effort and improving solution accuracy for complex geometries common in automotive structures. The primary material investigated in this study is extruded 6005 aluminium alloy.

IGA provides a promising alternative by employing CAD-based basis functions, such as NURBS or T-splines, for both geometry and the field approximation. In crash simulations, IGA allows exact representation of thin-walled components, curved structures, and solid bodies, improving the accuracy of stress and deformation predictions under high-impact loading. For shell-like structures, the precise geometric description captures bending and buckling behaviour more realistically, while for solid components, IGA provides accurate volumetric representation and stress distribution throughout the thickness.

The smoothness of IGA basis functions can improve the convergence characteristics of nonlinear dynamic simulations due to their higher-order continuity. Refinement strategies such as k-refinement enable local accuracy improvements without altering the overall geometry, making it possible to efficiently capture critical stress concentrations and deformation patterns in both thin-walled and solid regions [3, 6].

Despite these advantages, IGA introduces several challenges. It is generally more computationally expensive per degree of freedom than standard FE methods, and its integration into existing industrial crash solvers remains limited, particularly due to difficulties in incorporating CAD-based basis functions into established explicit dynamics frameworks.

In addition, while IGA improves geometric accuracy, its benefits may become less pronounced in highly nonlinear, contact, and fracture-dominated crash events, where solver robustness, material models, and failure criteria often govern the overall solution accuracy more strongly than geometric representation.

1.1 Objectives

The main objective of this thesis is to evaluate the applicability and maturity of IGA for crash simulation in automotive applications, with a focus on material anisotropy and its influence on crash behaviour through literature review and fracture surface evaluation. The work starts with simple material sample tests and gradually progresses to simulations of crash at the component level and full-vehicle level.

The material data for aluminium alloys is collected from strength tests and the generation of stress–strain curves using existing and newly measured data. IGA based simulation models are developed and analyzed under comparable loading conditions. The results are systematically compared with traditional FE models and available experimental data to assess the precision, robustness, and industrial feasibility of IGA.

The intended outcome is to determine whether the IGA is reliable and mature enough to support future implementation in automotive crash analysis at both component and assembly levels.

1.2 Limitations

This study is limited to:

- Evaluation of selected aluminium materials relevant to automotive structures.
- Crash simulations under defined loading scenarios (e.g., impact or quasi-static tests).
- Comparison with conventional FE methods using similar modeling assumptions.
- CAE and experimental validation within the available time and computational resources.
- Solid IGA model development using NURBS-based volumetric discretization.
- Full industrial implementation, large-scale optimization studies, and real-time crash simulations are outside the scope of this thesis.

1.3 Specification of the issue being investigated

The question being investigated is whether IGA can accurately and efficiently predict material and structural behaviour under crash loading conditions compared to traditional FE methods.

1. Can IGA accurately reproduce experimentally obtained stress–strain behaviour without tuning material parameters?
2. How does IGA perform in crash simulations at the component and assembly levels?
3. Does IGA offer advantages in terms of geometric representation, stress continuity, and computational efficiency?
4. How does IGA perform compared to traditional FE methods in terms of stress distribution, deformation patterns, and energy absorption?
5. What is the numerical robustness and convergence behaviour of IGA in nonlinear dynamic crash scenarios?
6. Is IGA sufficiently mature for practical implementation in automotive assembly-level crash analysis?

7. How do heat treatments affect the anisotropy and mechanical properties of extruded aluminium?

8. How do alloying elements influence the anisotropy and overall behaviour of extruded aluminium?

2

Theory

This section outlines the essential theoretical foundations of the IGA-based solid modelling framework.

2.1 Fundamentals of Numerical Methods

Numerical methods are essential for solving governing partial differential equations (PDEs) in solid mechanics, where analytical solutions are generally not feasible due to complex geometries, nonlinear material behaviour, and large deformation effects. In the crashworthiness analysis of extruded aluminium structures, discretisation-based approaches are required to approximate field variables such as displacement, stress, and strain over a finite computational domain.

The most widely used method in engineering is Finite Element Analysis (FEA), which discretises the geometry into FE and approximates the solution using piecewise polynomial shape functions. Although FEA is robust and computationally efficient, it introduces geometric approximation errors, particularly for curved and complex structures, and may require significant mesh refinement to achieve high accuracy leading to long and more expensive solutions [3].

IGA was developed to overcome these limitations by using CAD-based basis functions, such as NURBS, for both geometry representation and field approximation. This enables exact geometry representation and higher-order continuity, improving accuracy and convergence compared to traditional FEA [4, 6].

Both FEA and IGA are based on the weak formulation of the governing equations, but differ in how geometry and basis functions are treated. FEA relies on a separate meshing process, whereas IGA integrates design and analysis within a unified framework, reducing geometric inconsistencies and preprocessing effort [7].

In crash simulations of extruded aluminium components, FEA remains the industrial standard due to its maturity and efficiency, while IGA provides improved geometric fidelity and numerical accuracy, making it a promising alternative for high-fidelity structural analysis [3, 6].

2.1.1 Comparison of Theoretical Foundations of FEA and IGA

FEA and IGA are widely used numerical methods to solve engineering problems governed by partial differential equations. While FEA has been the dominant computational tool for several decades, IGA has emerged as a powerful alternative that addresses key limitations associated with geometry approximation and continuity in classical finite element formulations [3, 7]. IGA achieves higher-order continuity by employing spline-based basis functions such as NURBS or B-splines, enabling an exact representation of CAD geometry within the analysis framework.

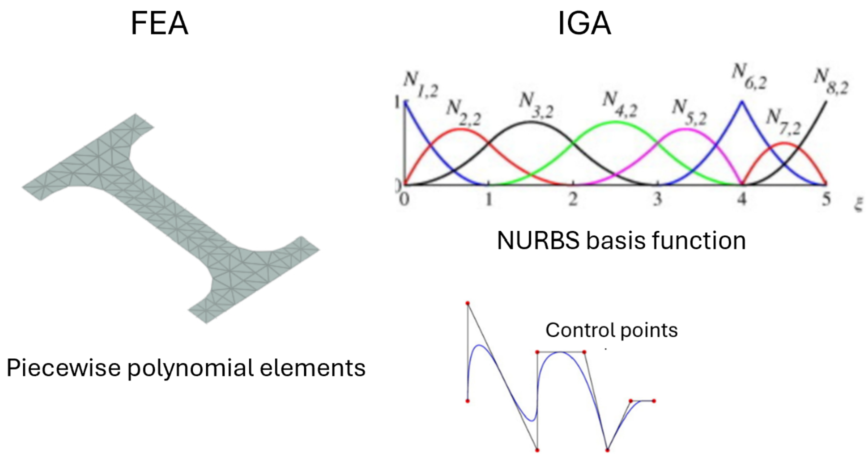

Figure 2.1: Comparison of classical FEA (Lagrange polynomial basis) and IGA (spline-based NURBS/B-spline basis functions) for geometry and field representation.

The fundamental differences between FEA and IGA are summarised in Table 2.1.

As shown in Table 2.1, the primary advantage of IGA lies in its ability to preserve exact geometry and provide higher-order continuity, which significantly improves numerical accuracy and convergence behaviour. These features are particularly beneficial in problems involving complex geometries and higher-order partial differential equations, where classical FEA may require additional computational effort to achieve similar accuracy [7].

Nevertheless, FEA remains the most widely used method in industrial applications due to its robustness, flexibility, and extensive software implementation. In contrast, IGA is increasingly being adopted in advanced computational mechanics applications where geometric fidelity and smooth solution fields are critical [3, 6].

In the context of this thesis on extruded aluminium structures, IGA is expected to improve stress prediction accuracy by more precisely capturing geometric features and enabling more efficient and faster solution procedures, while FEA serves as a benchmark for validation. This comparative approach allows a comprehensive

Table 2.1: Comparison between FEA and IGA

Aspect	**FEA**	**IGA**
Geometry Representation	Geometry is approximated and simplified using a piecewise polynomial elements, leading to discretisation errors	Exact geometry representation using CAD-based functions such as NURBS and B-splines [3]
Basis Functions	Lagrange polynomial basis functions with typically C^0 continuity	Spline-based basis functions (NURBS/B-splines) with higher-order continuity (C^1, C^2, etc.) [4]
Mesh Generation	Requires separate mesh generation and geometry cleanup	Eliminates traditional meshing by directly using CAD geometry [6]
Continuity	Limited inter-element continuity	High inter-element continuity enabling smooth solutions [7]
Accuracy	May require fine meshes to achieve high accuracy	Higher accuracy due to exact geometry and smooth basis functions [3]
Refinement Methods	Supports h- and p-refinement	Supports h-, p-, and k-refinement for improved convergence [7]
Higher-Order PDEs	Requires special formulations or mixed methods	Naturally suitable due to higher-order continuity [7]

assessment of both methods in predicting deformation and failure behaviour.

2.1.2 Volumetric Locking in Solid Formulations

Volumetric locking is a numerical issue in solid finite element formulations when modelling nearly incompressible materials, such as metals in plastic deformation or materials with Poisson's ratio approaching 0.5 [8, 9]. In such cases, the incompressibility constraint may be overly enforced at integration points, leading to an artificially stiff response and underestimated deformations.

This effect can result in inaccurate stress predictions, poor strain localisation, and convergence issues, particularly in bending-dominated and large deformation problems. Locking originates from displacement-based formulations where the same interpolation is used for displacement and strain, causing over-constrained volumetric deformation.

Additionally, volumetric locking may introduce spurious hydrostatic pressure oscillations, affecting stress triaxiality predictions. Since stress triaxiality is critical for ductile damage modelling, this can lead to inaccurate failure predictions [10]. To mitigate these issues, various techniques such as reduced integration, mixed formulations, enhanced strain methods, and stabilization approaches have been developed [8].

2.1.3 Isogeometric Analysis (IGA)

IGA is an advanced computational framework developed to bridge the long-standing *design-to-analysis gap* between Computer-Aided Design (CAD) and Finite Element Analysis (FEA). In conventional finite element methods, CAD geometries are approximated using piecewise polynomial elements, which may introduce geometric errors, particularly for curved surfaces and complex geometries. In contrast, IGA employs the same spline basis functions used in CAD-most commonly Non-Uniform Rational B-Splines (NURBS)-for both geometric representation and field variable approximation, thereby preserving the exact CAD geometry throughout the numerical analysis [3].

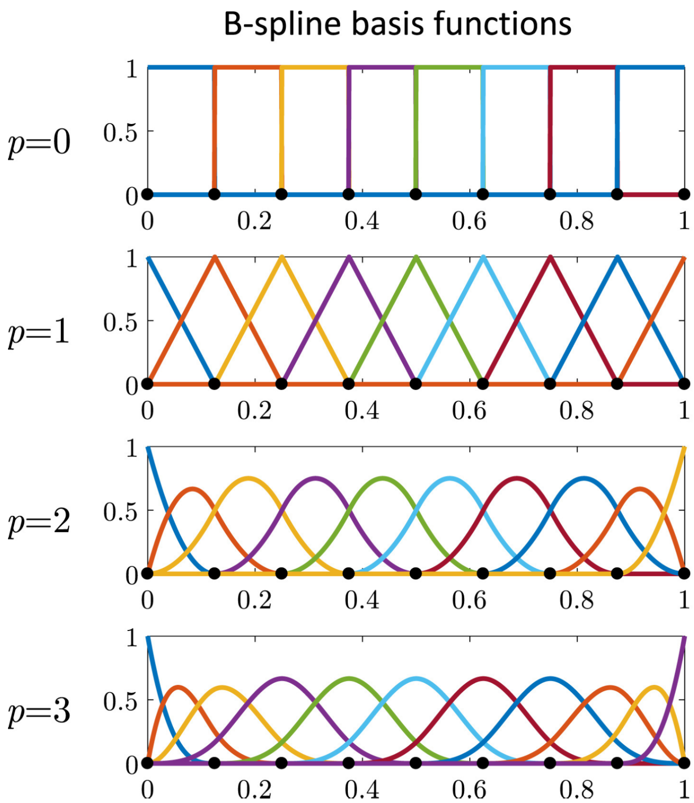

Figure 2.2: B-splines for $p = 1, 2, 3$, where the knots are indicated by black dots. Adapted from [1] with permission.

The fundamental concept of IGA is based on the use of smooth spline basis functions with higher-order continuity. Unlike classical FE, which typically possess only C^0 continuity across element boundaries, NURBS basis functions can achieve C^1, C^2, or higher continuity depending on the polynomial degree and knot multiplicity (Fig. 2.2). This enhanced smoothness improves the representation of deformation, stress gradients, and curvature effects, which is particularly beneficial in nonlinear structural mechanics and contact analyses.

A one-dimensional B-spline basis is recursively defined using a knot vector:

$$\mathcal{K} = \{\xi_1, \xi_2, \ldots, \xi_{n+k+1}\} \tag{2.1}$$

where k denotes the polynomial order and n is the number of basis functions. The B-spline basis functions are constructed recursively according to the Cox–de Boor formulation:

$$B_{r,k}(\xi) = \frac{\xi - \xi_r}{\xi_{r+k} - \xi_r} B_{r,k-1}(\xi) + \frac{\xi_{r+k+1} - \xi}{\xi_{r+k+1} - \xi_{r+1}} B_{r+1,k-1}(\xi) \tag{2.2}$$

with the zero-order basis functions defined as:

$$B_{r,0}(\xi) = \begin{cases} 1 & \text{if } \xi_r \leq \xi < \xi_{r+1} \\ 0 & \text{otherwise} \end{cases} \tag{2.3}$$

Fig. 2.3 illustrates quadratic B-spline basis functions and their corresponding derivatives for an open knot vector. The continuity of the derivatives across knot spans demonstrates the smoothness characteristics of spline discretizations. In one-dimensional spline spaces, the nonzero knot spans define the elements, while the continuity across element boundaries is governed by the knot multiplicity. In general, spline basis functions exhibit C^{k-m} continuity, where k is the polynomial order and m is the knot multiplicity.

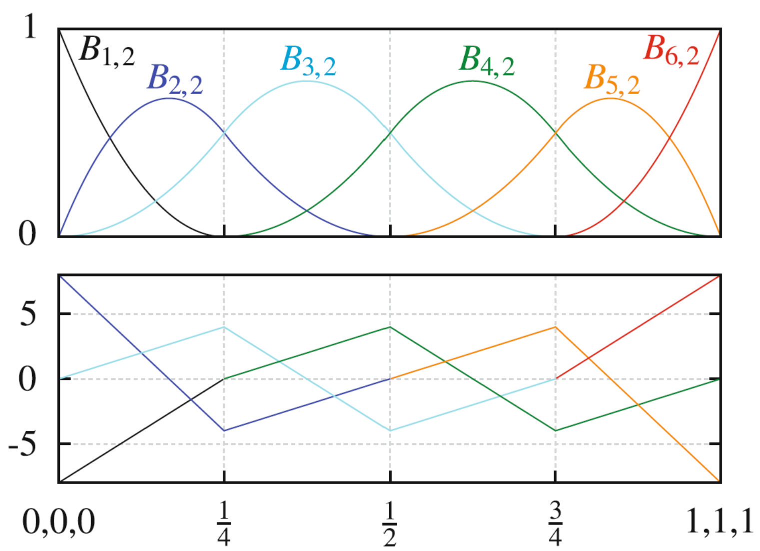

Figure 2.3: Quadratic B-spline basis functions and their derivatives for an open knot vector [2].

NURBS basis functions are obtained through a weighted normalization of the B-spline basis functions:

$$N^i(\xi) = \frac{w^i B^i(\xi)}{\sum_j w^j B^j(\xi)} \tag{2.4}$$

where w^i denotes the associated control point weights. If all weights are equal to unity, the formulation reduces to standard B-splines. The geometry representation is then expressed as:

$$\mathbf{x}(\xi) = \sum_{i=1}^{n} R_i(\xi)\mathbf{P}_i \tag{2.5}$$

where $R_i(\xi)$ are the NURBS basis functions and $\mathbf{P}_i$ are the control points defining the geometry. Unlike classical finite element interpolation, spline approximations are generally non-interpolatory, meaning that the control points do not necessarily lie on the geometry itself. Consequently, the imposition of Dirichlet boundary conditions may require weak enforcement techniques.

Higher-dimensional spline basis functions are constructed through tensor products of one-dimensional basis functions. For example, a two-dimensional spline basis can be obtained by combining one-dimensional basis functions in the parametric directions ξ and η:

$$B^i(\xi, \eta) = B_{r,k_1}(\xi)\, B_{s,k_2}(\eta) \tag{2.6}$$

where k_1 and k_2 represent the polynomial orders in each parametric direction. Fig. 2.4 illustrates the construction of a two-dimensional B-spline basis function through the tensor product of quadratic and cubic one-dimensional spline functions. In multidimensional spline discretizations, the number of active basis functions per element is obtained from the product of the active basis functions in each parametric direction.

The same spline basis functions used for geometry representation are also employed to approximate unknown field variables, ensuring consistency between geometry and analysis. This unified representation significantly improves numerical accuracy and convergence behaviour compared to conventional finite element formulations [4]. Furthermore, the exact geometric description provided by NURBS is particularly advantageous in contact mechanics applications, where smooth surface representation is essential for accurate sliding contact behaviour (see Fig. 2.5).

The inherent smoothness of NURBS basis functions enables IGA to naturally handle problems involving higher-order partial differential equations, such as Kirchhoff–Love plate and shell theories, without introducing additional rotational degrees of freedom or specialised formulations. As a result, IGA provides improved convergence rates,

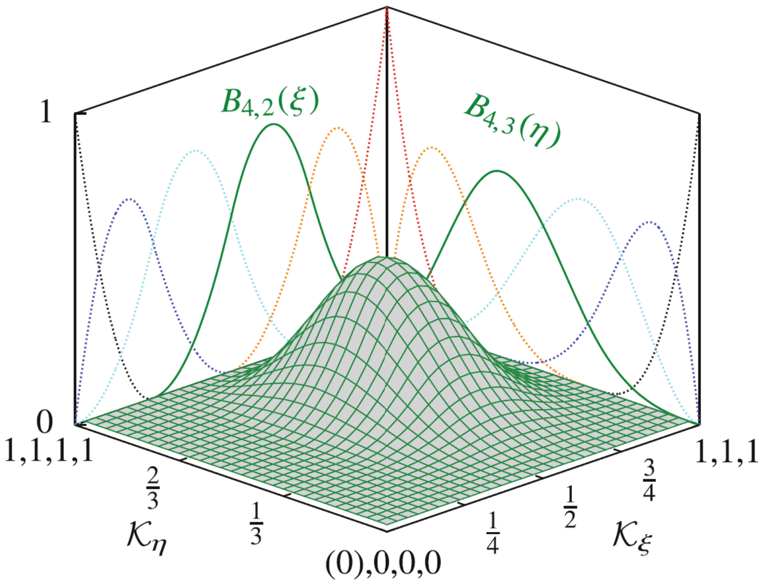

Figure 2.4: Construction of a two-dimensional B-spline basis function using the tensor-product formulation [2].

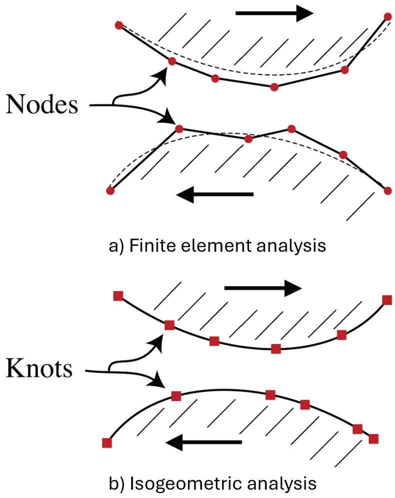

Figure 2.5: Sliding contact representation. (a) Faceted polynomial FE may introduce inaccuracies in sliding contact, whereas (b) NURBS-based geometries provide smooth and accurate surface descriptions [3].

enhanced stress prediction capability, and superior geometric fidelity for complex nonlinear structural analyses [7].

2.1.4 IGA Refinement Techniques

Refinement strategies in IGA are essential for improving numerical accuracy while preserving the exact geometric representation provided by Non-Uniform Rational B-Splines (NURBS). In contrast to classical finite element methods, where mesh refinement alters the geometric discretization, IGA enables refinement directly at the level of spline basis functions without modifying the underlying geometry. The main refinement strategies in IGA are h-refinement, p-refinement, and k-refinement, and their combinations define the so-called $hp\kappa$-refinement space [3, 11].

- **h-Refinement (Knot Insertion)**

  h-refinement is achieved through knot insertion, where new knot values are introduced into the existing knot vector, resulting in a subdivision of the parametric domain into smaller elements. This increases the number of elements and control points while preserving the exact geometry of the NURBS representation. The element size h is reduced while polynomial degree p and smoothness characteristics remain unchanged.

- **p-Refinement (Degree Elevation)**

  p-refinement corresponds to increasing the polynomial degree p of the spline basis functions while keeping the geometry fixed. This enhances approximation accuracy and smoothness without modifying the geometric representation. Proper adjustment of knot multiplicities ensures geometric invariance during degree elevation.

- **k-Refinement (Smoothness-Preserving Refinement)**

  k-refinement is obtained by combining degree elevation and knot insertion. It increases both polynomial order and inter-element continuity, typically achieving C^{p-1} smoothness. This diagonal refinement path in the $hp\kappa$-space leads to higher accuracy with fewer degrees of freedom compared to classical finite element approaches.

- **Combined Refinement Strategies**

  The refinement space allows flexible transitions between h-, p-, and k-refinement strategies. As illustrated in Fig. 2.6, pure h-refinement reduces element size, pure p-refinement increases polynomial order, and knot repetition controls continuity without changing geometry. The combination of these strategies enables traversal of the full refinement space, offering a balance between accuracy, smoothness, and computational cost.

In LS-DYNA IGA, refinement is defined using the `*IGA_REFINE_SOLID` keyword, where the parameter `rtyp` specifies the refinement strategy. Here, `rtyp = 1` corre-

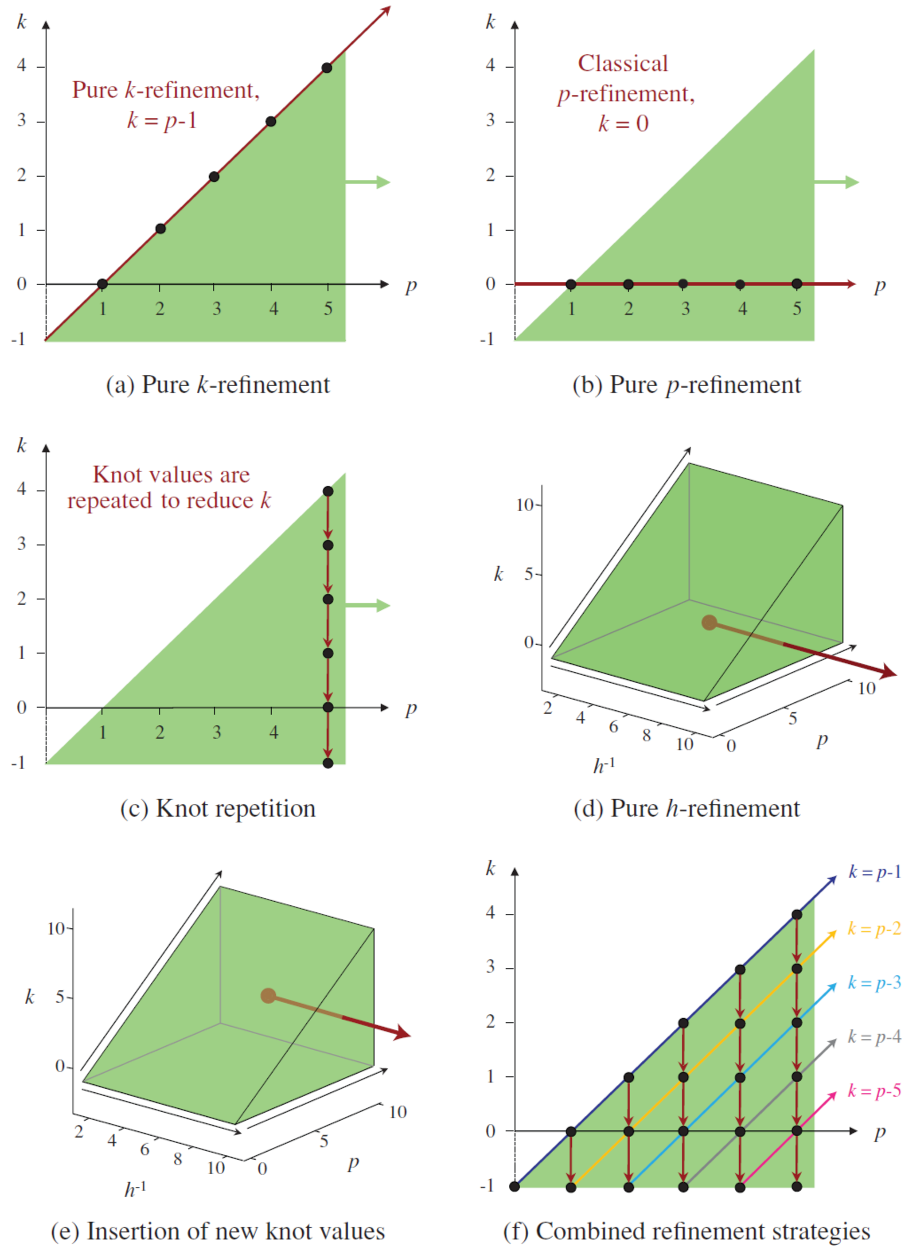

(a) Pure k-refinement (b) Pure p-refinement
(c) Knot repetition (d) Pure h-refinement
(e) Insertion of new knot values (f) Combined refinement strategies

Figure 2.6: Refinement strategies in the $hp\kappa$-space: (a) pure k-refinement, (b) pure p-refinement, (c) knot repetition, (d) pure h-refinement, (e) insertion of new knot values, and (f) combined refinement strategies [4].

sponds to p-refinement (degree elevation), `rtyp = 2` represents h-refinement (knot insertion), and `rtyp = 3` defines k-refinement, which combines degree elevation with increased continuity of the NURBS basis functions. These refinement approaches improve numerical accuracy while preserving the exact CAD geometry representation of the IGA model [12].

2.1.5 Hybrid Approaches: Coupling FEA and IGA

Hybrid FEA–IGA approaches combine the geometric accuracy and higher-order continuity of IGA with the computational efficiency and robustness of conventional FEA. This enables accurate and practical simulations for complex engineering systems where different regions require varying modelling fidelity.

In such frameworks, IGA is applied to critical regions with high stress gradients, curvature, or geometric sensitivity (e.g., fillets, joints, and contact zones), while conventional FE are used in less critical areas to reduce computational cost [3, 7]. LS-DYNA supports this FEA–IGA hybridization by allowing spline-based elements to be integrated into standard finite element models, enabling localized refinement without full-domain discretisation.

Coupling between FEA and IGA domains is achieved through interface techniques such as mortar methods, Nitsche-type formulations, and domain decomposition, ensuring displacement compatibility and accurate transfer of stresses and strains across regions [6, 7]. However, special attention is required due to the differing continuity levels (C^0 in FEA vs. C^1 or higher in IGA).

At the assembly level, FEA–IGA hybrid modelling is particularly effective for structures such as automotive components, where critical regions involving buckling, large deformation, or fracture can be modelled using IGA, while the remaining structure is efficiently handled using FEA.

Overall, hybrid FEA–IGA approaches improve geometric representation, numerical accuracy, and convergence behaviour, while maintaining computational efficiency and enabling closer integration between CAD and analysis [3, 6, 13]. In this study, such a hybrid strategy is employed to accurately predict deformation and fracture behaviour in extruded aluminium assemblies.

2.1.6 Interpolation and Background Meshes in LS-DYNA IGA

In the LS-DYNA implementation of IGA, the exact geometry is represented using NURBS basis functions. In addition to this exact representation, an interpolation mesh is introduced to support model definition and visualization. This mesh consists of a faceted approximation of the geometry composed of elements that represent the underlying NURBS description [14]. It is used to position material, define contact interfaces, and provide a visualization framework for post-processing, enabling the use of standard LS-DYNA post-processors without requiring specialised tools.

For numerical integration in trimmed and immersed IGA formulations, a background finite element mesh is employed. Although the geometry is defined exactly by NURBS functions, the governing equations are evaluated on this background mesh, which provides the integration cells and Gauss quadrature points required for the computation of stiffness matrices, internal forces, stresses, and other state variables.

The introduction of the background mesh is motivated by the difficulty of performing direct integration over trimmed NURBS geometries in a robust and computationally efficient manner. To overcome this, LS-DYNA embeds the CAD geometry into a structured computational domain, where the background mesh defines the integration regions without requiring a body-fitted finite element discretization, while preserving the exact NURBS-based geometry representation.

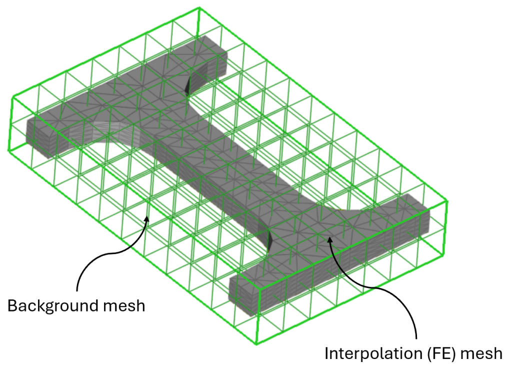

Figure 2.7: Schematic representation of interpolation mesh and background mesh in LS-DYNA IGA. The interpolation mesh is used for geometry representation, material assignment, and visualization, while the background mesh provides numerical integration points.

Within this framework, there is a clear separation between geometry representation and numerical computation. As illustrated in Fig. 2.7, the interpolation mesh is responsible for geometry-related tasks, including material assignment, contact definition, and visualization, whereas the background mesh is used exclusively for numerical integration and evaluation of the governing equations. This separation enhances modelling flexibility, simplifies the treatment of complex geometries, and enables mesh refinement through modification of the background discretization without altering the underlying CAD model [14].

2.2 IGA and Explicit Time Integration

In conventional FEM, shell and solid discretizations commonly employ triangular, quadrilateral, tetrahedral, and hexahedral elements. Lower-order elements, particularly linear triangular elements, can exhibit excessive stiffness in bending-dominated problems due to constant strain assumptions, and require finer meshes to accurately capture deformation behaviour [15]. In contrast, spline-based IGA formulations achieve greater continuity and improved numerical performance with fewer degrees of freedom [3].

For three-dimensional applications, IGA spline-based solid formulations are constructed analogously to hexahedral FE while maintaining an exact geometric representation. This makes IGA particularly suitable for structural mechanics, crashworthiness, and fracture simulations involving complex geometries and large deformations [4].

2.2.1 Explicit Time Integration

Explicit time integration methods are widely used for highly nonlinear dynamic problems such as crash and impact simulations because they avoid iterative solution procedures and do not require inversion of a global stiffness matrix at each time increment [16].

The semi-discrete equation of motion is expressed as

$$\mathbf{M}\ddot{\mathbf{u}} + \mathbf{f}_{\text{int}}(\mathbf{u}) = \mathbf{f}_{\text{ext}} \tag{2.7}$$

where $\mathbf{M}$ is the mass matrix, $\ddot{\mathbf{u}}$ is the nodal acceleration vector, $\mathbf{f}_{\text{int}}$ represents the internal force vector, and $\mathbf{f}_{\text{ext}}$ denotes the external force vector.

The central difference method is commonly used for explicit time integration. The displacement update equation is given by

$$\mathbf{u}^{n+1} = 2\mathbf{u}^{n} - \mathbf{u}^{n-1} + \Delta t^2 \mathbf{M}^{-1} \left(\mathbf{f}_{\text{ext}}^{n} - \mathbf{f}_{\text{int}}^{n}\right) \tag{2.8}$$

where Δt is the time increment.

The use of a lumped mass matrix significantly improves computational efficiency, since matrix inversion becomes trivial. This makes explicit formulations highly suitable for large-scale nonlinear analyses involving contact, material nonlinearity, and fracture [16].

However, explicit methods are conditionally stable and require the time step to remain below a critical value governed by the Courant-Friedrichs-Lewy (CFL) stability criterion:

$$\Delta t_{\text{crit}} = \frac{L}{c} \tag{2.9}$$

where L is the characteristic element length and c is the material wave speed.

For isotropic elastic solids, the wave speed is expressed as

$$c = \sqrt{\frac{E}{\rho(1-\nu^2)}} \tag{2.10}$$

where E is Young's modulus, ρ is the material density, and ν is Poisson's ratio.

In IGA formulations, the stable time increment is additionally influenced by spline order and knot span size. Higher-order NURBS basis functions improve smoothness and solution accuracy but may reduce the stable time step due to increased spectral properties of the discretised system [17]. Consequently, refinement strategies such as *h*-, *p*-, and *k*-refinement directly influence computational efficiency and numerical stability in explicit IGA simulations.

To improve implementation efficiency, Bézier extraction techniques are commonly employed to integrate NURBS-based IGA formulations into conventional finite element solver architectures [13]. Furthermore, explicit solvers may use mass scaling techniques to increase the stable time increment by modifying the element density while maintaining an acceptable solution accuracy [16].

2.2.2 Influence of IGA on Solver Performance

The use of IGA significantly influences the numerical performance of explicit solvers such as LS-DYNA due to the higher-order continuity and smoothness of NURBS basis functions. Compared to conventional finite element discretizations, IGA basis functions possess increased inter-element continuity, typically ranging from C^0 to C^{p-1} continuity, where p is the polynomial degree [3, 4]. This improved smoothness enhances the accuracy of stress and strain fields while reducing numerical oscillations and locking phenomena.

In explicit dynamic analysis, solver performance is strongly governed by the spectral properties of the discretised system. Due to the higher continuity of spline basis functions, IGA formulations generally exhibit improved wave propagation characteristics and lower numerical dispersion errors compared to standard FEM [17]. This is particularly advantageous in crashworthiness and impact simulations where accurate stress wave transmission is essential.

However, the increased continuity and higher-order basis functions also influence the stability limits of the explicit solver. In IGA, the critical time step depends not only on the smallest knot span but also on the polynomial order and continuity of the spline basis. Higher-order NURBS discretizations tend to increase the maximum eigenfrequency of the system, which may reduce the stable time increment compared to conventional low-order FE [18].

To improve computational efficiency, LS-DYNA employs lumped mass matrices and diagonalized system formulations in explicit IGA implementations. This allows the equations of motion to be solved efficiently without iterative matrix inversion while preserving the advantages of spline-based discretizations [16]. Additionally, Bézier extraction techniques are commonly used to integrate NURBS-based IGA formulations into existing finite element solver architectures. Bézier extraction converts spline basis functions into Bernstein polynomial representations, enabling efficient implementation within standard FEM data structures and element routines [13].

Another important advantage of IGA in explicit solvers is the improved geometric exactness inherited directly from CAD models. Since NURBS geometries are represented exactly, geometric approximation errors commonly present in conventional FEM meshes are eliminated. This improves contact accuracy, stress prediction, and structural response in nonlinear simulations involving large deformations and complex geometries [3].

Furthermore, refinement strategies such as k-refinement allow IGA models to achieve high solution accuracy with fewer degrees of freedom than traditional FEM discretizations. This can significantly reduce computational cost while maintaining superior convergence behaviour and smooth solution fields [4].

2.3 Anisotropy in Metallic Materials

Anisotropy in metallic materials refers to the directional dependence of mechanical properties arising from microstructural evolution and crystallographic texture developed during thermomechanical processing operations such as rolling, extrusion, and forming. In extruded aluminium alloys, severe plastic deformation during manufacturing causes grain elongation and preferred crystallographic orientations, resulting in orthotropic material behaviour. Consequently, the mechanical response of the material, including elastic stiffness, yield strength, ductility, and fracture characteristics, varies with loading direction.

For isotropic materials, yielding is commonly described using the von Mises yield criterion, which assumes identical material behaviour in all directions. However, this assumption is insufficient for anisotropic materials such as extruded aluminium alloys, where directional dependency significantly influences plastic deformation and failure behaviour. Therefore, anisotropic constitutive models and yield criteria are required to accurately represent the directional response of the material under multiaxial loading conditions.

The elastic constitutive behaviour of anisotropic materials is generally expressed using the generalized Hooke's law:

$$\sigma_{ij} = C_{ijkl}\,\varepsilon_{kl} \tag{2.11}$$

where σ_{ij} and ε_{kl} denote the stress and strain tensors, respectively, and C_{ijkl} represents the fourth-order anisotropic stiffness tensor governing the directional elastic response of the material.

2.3.1 Lankford Parameter R-Value and Plastic Anisotropy

Plastic anisotropy in sheet metals and extruded alloys is commonly characterised using the Lankford parameter, also referred to as the R-value [19]. The R-value describes the resistance of a material to thickness reduction during plastic deformation and is defined as the ratio of the plastic strain in the width direction to that in the thickness direction during uniaxial tensile loading:

$$R = \frac{\varepsilon_w^p}{\varepsilon_t^p} \tag{2.12}$$

where ε_w^p and ε_t^p are the plastic strains in the width and thickness directions, respectively.

Assuming plastic incompressibility during deformation, the plastic strain components satisfy

$$\varepsilon_l^p + \varepsilon_w^p + \varepsilon_t^p = 0 \tag{2.13}$$

where ε_l^p denotes the longitudinal plastic strain in the loading direction.

The anisotropic behaviour of metallic materials is further characterised using the average normal anisotropy and planar anisotropy parameters. The average normal anisotropy, $\bar{R}$, represents the overall resistance of the material to thinning and is associated with deep drawability. It is expressed as

$$\bar{R} = \frac{R_0 + 2R_{45} + R_{90}}{4} \tag{2.14}$$

where R_0, R_{45}, and R_{90} correspond to the measured R-values at orientations of 0°, 45°, and 90° relative to the rolling or extrusion direction.

The planar anisotropy, ΔR, characterizes the variation of plastic flow behaviour within the plane of the material and is given by

$$\Delta R = \frac{R_0 - 2R_{45} + R_{90}}{2} \tag{2.15}$$

Planar anisotropy is closely related to non-uniform deformation during forming operations and is often associated with defects such as earing in deep-drawn components. A lower value of ΔR indicates more uniform in-plane deformation behaviour and improved forming performance.

Therefore, the R-value, average normal anisotropy, and planar anisotropy are important parameters for evaluating the formability, directional deformation characteristics, and plastic flow behaviour of anisotropic metallic materials.

2.3.2 Tsai–Hill Anisotropic Yield Criterion

The Tsai–Hill criterion is widely used to model orthotropic yielding behaviour in anisotropic materials. For plane stress conditions, the yield function is expressed as

$$\frac{\sigma_1^2}{X^2} - \frac{\sigma_1\sigma_2}{X^2} + \frac{\sigma_2^2}{Y^2} + \frac{\tau_{12}^2}{S^2} = 1 \tag{2.16}$$

where σ_1 and σ_2 are the normal stresses in the principal material directions, τ_{12} is the in-plane shear stress, and X, Y, and S are the directional yield strengths.

For a general three-dimensional stress state, the criterion becomes

$$\left(\frac{\sigma_1}{X}\right)^2 + \left(\frac{\sigma_2}{Y}\right)^2 + \left(\frac{\sigma_3}{Z}\right)^2 - \frac{\sigma_1\sigma_2}{X^2} - \frac{\sigma_2\sigma_3}{Y^2} - \frac{\sigma_3\sigma_1}{Z^2} + \frac{\tau_{12}^2}{S_{12}^2} + \frac{\tau_{23}^2}{S_{23}^2} + \frac{\tau_{31}^2}{S_{31}^2} = 1 \tag{2.17}$$

The Tsai–Hill model accounts for directional differences in yielding and is therefore more suitable for anisotropic aluminium alloys than isotropic yield criteria.

Advanced anisotropic yield models, such as Hill's 1948 criterion and Barlat yield functions, have also been developed to improve prediction accuracy under multiaxial loading conditions.

2.4 Material Triaxiality and Ductile Fracture

Stress triaxiality is a fundamental parameter in ductile fracture mechanics because it describes the influence of the stress state on void growth and failure. It is defined as the ratio of hydrostatic stress to equivalent von Mises stress:

$$\eta = \frac{\sigma_m}{\sigma_{eq}}, \qquad \sigma_m = \frac{1}{3}(\sigma_1 + \sigma_2 + \sigma_3) \tag{2.18}$$

High triaxiality promotes void growth and early fracture, whereas low triaxiality corresponds to shear-dominated deformation with delayed failure [20, 21].

The von Mises equivalent stress is expressed as

$$\sigma_{eq} = \sqrt{\frac{1}{2}\left[(\sigma_1 - \sigma_2)^2 + (\sigma_2 - \sigma_3)^2 + (\sigma_3 - \sigma_1)^2\right]} \tag{2.19}$$

The equivalent plastic strain is commonly expressed as

$$\epsilon_{eq} = \frac{\sqrt{2}}{3}\sqrt{(\epsilon_1 - \epsilon_2)^2 + (\epsilon_2 - \epsilon_3)^2 + (\epsilon_3 - \epsilon_1)^2} \tag{2.20}$$

Under plane stress conditions, stress triaxiality can be estimated using the strain ratio parameter

$$\beta = \frac{\epsilon_{yy}}{\epsilon_{xx}} \tag{2.21}$$

leading to

$$\eta = \frac{1 + \beta}{3\sqrt{1 - \beta + \beta^2}} \tag{2.22}$$

For notched specimens, Bridgman proposed a correction to account for geometric constraint effects:

$$\eta = \frac{1}{3} + \ln\left(1 + \frac{a}{2R}\right) \tag{2.23}$$

where a is the minimum cross-sectional radius and R is the curvature radius in the necked region [22].

2.4.1 Johnson–Cook Fracture Model

The Johnson–Cook fracture model defines the equivalent fracture strain as:

$$\varepsilon_f = \left(D_1 + D_2 e^{D_3 \sigma^*}\right)\left(1 + D_4 \ln \dot{\varepsilon}^*\right)\left(1 + D_5 T^*\right)$$

where $\sigma^* = \sigma_m/\sigma_{eq}$ is stress triaxiality, $\dot{\varepsilon}^*$ is the normalized strain rate, and T^* is the homologous temperature [23].

Damage evolution is accumulated as:

$$D = \sum \frac{\Delta \varepsilon_p}{\varepsilon_f}$$

Fracture occurs when $D = 1$.

2.4.2 Cockcroft–Latham Criterion

The Cockcroft-Latham criterion suggests that a fracture usually occurs at maximum tensile stress.

$$C = \int_0^{\varepsilon_f} \sigma_1 \, d\varepsilon_p = C_{crit}$$

where σ_1 is the maximum principal stress and C_{crit} is a material constant [24].

This simple energy-based formulation is widely used in metal forming simulations due to its computational efficiency and easy calibration procedure. Although more advanced failure criteria have been developed, the model remains advantageous due to its simplicity and robustness, as discussed in previous master's thesis work [25], and was therefore included in the present study.

2.5 GISSMO Damage Model

The Generalized Incremental Stress State dependent damage Model (GISSMO) is a phenomenological damage framework widely used for predicting ductile fracture under complex loading conditions [26]. Rather than acting as a standalone fracture criterion, GISSMO provides a damage evolution formulation in which various failure criteria can be incorporated. The scalar damage variable D is defined within the interval

$$0 \leq D \leq 1, \tag{2.24}$$

where $D = 0$ denotes the undamaged material state and $D = 1$ corresponds to complete material failure.

Damage evolution is expressed incrementally as

$$\Delta D = n D^{1-\frac{1}{n}} \frac{\Delta \varepsilon_p}{\varepsilon_f} \tag{2.25}$$

and can be integrated as

$$D = \left(\frac{\varepsilon_p}{\varepsilon_f} \right)^n \tag{2.26}$$

where ε_f is the failure strain and n is the damage exponent.

The GISSMO model also introduces an instability parameter F to describe material softening and localization:

$$\Delta F = nF^{1-\frac{1}{n}} \frac{\Delta \varepsilon_p}{\varepsilon_{p,\mathrm{loc}}} \tag{2.27}$$

Once instability is reached, stress degradation is described by

$$\sigma_{\mathrm{true}} = \sigma_{\mathrm{eff}} \left[1 - \left(\frac{D - D_{\mathrm{crit}}}{1 - D_{\mathrm{crit}}} \right)^m \right] \tag{2.28}$$

where m is the fading exponent controlling stress degradation.

GISSMO is commonly coupled with constitutive plasticity models such as Johnson–Cook, Cockcroft–Latham and advanced anisotropic plasticity formulations to improve prediction of ductile failure in metallic structures subjected to complex loading paths.

2.6 Material Behaviour of Extruded Aluminium

Al–Mg–Si (6xxx series) aluminium alloys are widely used in automotive structural and crash-relevant applications due to their high specific strength, good ductility, corrosion resistance, and energy absorption capability [27]. In extruded form, these alloys are widely used in load-bearing automotive applications, including bumper beams, side impact structures, and other energy-absorbing structural components.

From a material mechanics perspective, the extrusion process induces significant plastic deformation, leading to elongated grain structures and the development of crystallographic texture along the extrusion direction. As a result, extruded aluminium alloys exhibit anisotropic mechanical behaviour, where strength and deformation response depend on the loading orientation [28]. This anisotropy is particularly relevant under crash loading conditions, where multiaxial stress states promote strain localization and direction-dependent damage evolution.

The mechanical response of Al–Mg–Si alloys is primarily governed by precipitation hardening. During artificial ageing, Mg_2Si precipitates form and hinder dislocation motion, thereby increasing strength and work-hardening capacity [29, 30]. In addition, alloying elements such as Mn and Fe influence microstructural evolution. Mn contributes to the formation of dispersoids that stabilize the microstructure and suppress recrystallization, while Fe-rich intermetallic particles may act as stress concentrators and potential initiation sites for damage.

Among the 6xxx series, 6005A-T6 is commonly used in automotive extrusion profiles due to its balanced mechanical properties and good extrudability. Its response is strongly influenced by the processing history and exhibits clear anisotropic characteristics associated with the extrusion direction. The T6 temper condition indicates that the alloy has undergone a solution heat treatment, quenching, and artificial ageing, resulting in precipitation-hardened microstructures that provide the required strength–ductility balance for structural applications.

To understand the influence of alloy composition on anisotropic material behaviour, 6082-T6 is also considered in the broader context of 6xxx alloys. Compared to 6005A, 6082 contains a higher Mg and Si content, resulting in a stronger precipitation hardening response and higher strength levels. This makes it a relevant reference material for assessing how variations in alloy chemistry affect anisotropy, texture development, and deformation resistance in extruded aluminium structures.

3

Methods

This section briefly outlines the methodology used to evaluate the IGA-based solid model under various loading conditions.

3.1 IGA Analysis

3.1.1 IGA-Based Computational Modelling Framework

IGA was implemented using two different modelling approaches. Both approaches are based on the same fundamental concept, in which the geometry and the solution fields are represented using identical spline basis functions. This ensures consistency between the geometric description and the numerical analysis. The main difference between the approaches lies in the modelling workflow and the way the geometry is constructed and visualised. The Box method is primarily a text-based, file-driven approach, whereas the ANSA method is a geometry-based, visual pre-processing approach.

The Box method is based on a structured parametric domain in which the geometry is represented using tensor-product NURBS (Non-Uniform Rational B-Splines). In this formulation, the IGA model is defined through an include file that contains all necessary spline information, including control points, knot vectors, trimming data, and refinement parameters associated with the coordinate-defined structure. In this approach, the IGA representation is typically generated from a pre-existing FE discretisation, which is then mapped into the spline-based parametric formulation. The following LS-DYNA IGA keywords were used within the include file to define the spline-based solid representation:

```
*PART
*SECTION_IGA_SOLID
*IGA_DEV_VOLUME_XYZ
*IGA_SOLID
*IGA_3D_NURBS_XYZ
*IGA_REFINE_SOLID
```

The *IGA_REFINE_SOLID keyword is applicable only to models generated using the Box Method, as the current ANSA implementation does not support refinement via this keyword. Instead, NURBS-based refinement was carried out directly within ANSA during preprocessing by modifying the control point discretisation at the preprocessing stage prior to export.

A consistent part identification number (PID) was assigned across all corresponding IGA definitions to ensure a coherent mapping between geometry, section properties, and refinement data. In contrast to conventional finite element discretisations, the trimmed parametric representation enables local geometric refinement while preserving the inherent higher-order continuity of the NURBS basis functions.

The Box method provides several advantages, including direct geometric refinement through knot insertion and degree elevation, smooth representation of complex geometries with higher-order continuity, consistent coupling between geometry and solution fields, and improved geometric accuracy compared with standard FE mesh discretisations.

The ANSA method follows the same IGA formulation but uses the commercial pre-processing tool ANSA to construct, visualise, and manage the spline-based geometry in a more interactive environment. In this approach, the geometry can be directly defined and discretised within ANSA, where an interpolation finite element mesh is generated and subsequently used as the basis for constructing the IGA representation. This enables the spline-based model to be derived directly from the geometric definition without requiring a fully pre-existing meshed model in the same manner as the Box approach.

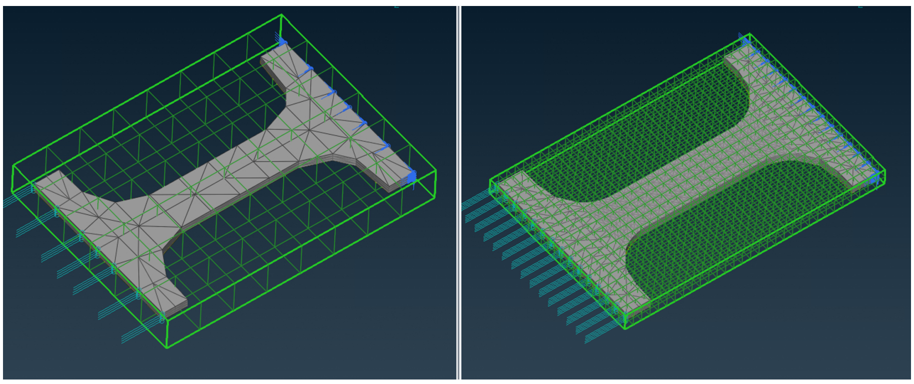

Figure 3.1: Visual representation of a NURBS-based IGA model in ANSA, showing coarse and fine discretizations.

A key advantage of the ANSA-based approach is its integration within industrial preprocessing workflows and its ability to handle complex geometries in a graphical environment. The spline patches are visualised in a mesh-like format, which improves interpretability and facilitates model verification prior to analysis, as illustrated in Fig. 3.1. Although the modelling environments differ, both approaches are consistent in their underlying IGA formulation and ensure a unified representation of geometry and analysis throughout the simulation process.

3.2 IGA Assessment Methodology

A hierarchical validation strategy was adopted to evaluate the accuracy and robustness of the proposed IGA based solid modeling framework. The methodology follows the conventional automotive structural development pyramid, progressing from simple coupon-scale specimens to increasingly complex structural systems. As illustrated in Fig. 3.2, this multi-level validation approach ensures that the predictive capability of the IGA framework is systematically assessed before its application to large-scale vehicle structures.

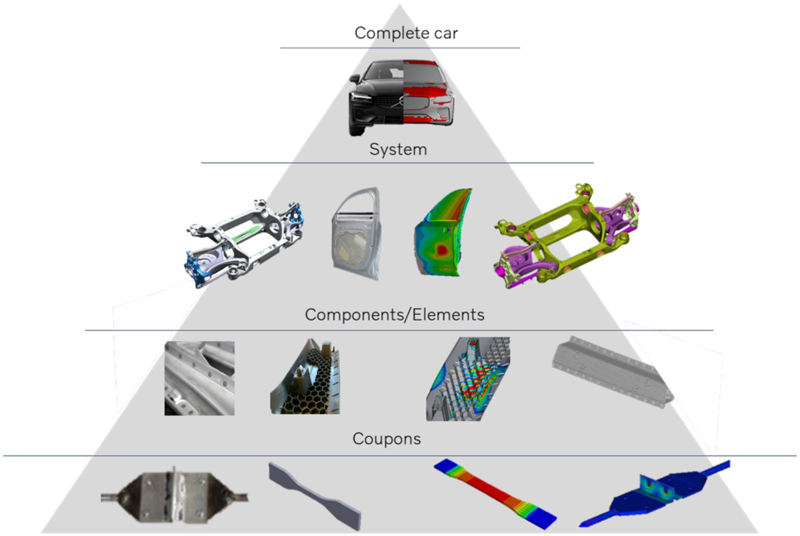

Figure 3.2: Hierarchical validation strategy for the proposed IGA framework, progressing from coupon-level to component, assembly, and full vehicle-level.

The validation process begins at the **coupon-level**, where standardized tensile and shear specimens are analyzed to verify the material representation, constitutive behaviour, and local deformation response. Numerical predictions are compared with experimental measurements and conventional finite element (FE) simulations through force–displacement responses and failure characteristics.

The second stage focuses on the **component-level**, where individual structural parts representative of automotive applications are investigated. At this level, the ability of the IGA model to accurately capture stiffness, stress distributions, strain localization, and deformation patterns is assessed.

Subsequently, **assembly-level** analyses are performed by combining multiple components into realistic substructures. These simulations evaluate load transfer mechanisms, component interactions, contact, joint behaviour, and the overall structural response of complex assemblies.

Finally, the methodology is extended towards the full vehicle level, where the framework is embedded within a global FE model to assess its applicability under representative crash conditions.

This hierarchical validation procedure establishes confidence in the proposed IGA framework across multiple length scales, ensuring reliable performance from material characterization at the coupon level to full vehicle structural analysis.

3.2.1 Coupon-Level Validation

To validate the predictive capability of the numerical framework at the material level, a comprehensive coupon-level testing programme was conducted. The investigated material system is based on aluminium alloy 6005A-T6, which is widely used in automotive structural applications due to its favourable combination of strength, ductility, and extrudability. However, since extruded 6xxx-series alloys exhibit pronounced anisotropic behaviour induced by texture evolution during processing, 6082-T6 is additionally considered as a comparative material to evaluate the influence of alloy composition on anisotropic response and fracture behaviour under varying loading conditions.

The nominal chemical composition and typical mechanical properties of 6005A-T6 used in structural extrusion applications are summarized in Tables 3.1 and 3.2, respectively.

Table 3.1: Chemical compositions of the investigated aluminium alloys (wt.%), SS-EN 573-3:2013 (E).

Alloy	Cr	Cu	Fe	Mg	Mn	Si	Ti	Zn	Al
6005A-T6	0.30	0.30	0.35	0.40–0.7	0.50	0.50–0.9	0.10	0.20	Rem.
6082-T6	0.25	0.10	0.50	0.6–1.2	0.4–1.0	0.7–1.3	0.10	0.20	Rem.

Table 3.2: Typical mechanical properties of aluminium alloy 6005A-T6.

Property	Yield Str. (MPa)	Ultimate Str. (MPa)	Elongation (%)	Elastic Modulus (GPa)	Density (kg/m^3)
6005A-T6	245–260	260–300	9–11	70	2700

Uniaxial tensile tests were performed using standard and large-scale specimens to characterise the elastic–plastic response and capture strain localisation effects as well as potential size-dependent behaviour. Shear behaviour was investigated using 45° and 90° shear configurations, representing combined and near-pure shear stress states, respectively, to evaluate the material response under shear-dominated deformation modes.

Notched tensile specimens were employed to promote stress concentration and investigate damage initiation under non-uniform stress states. In addition, punch tests were conducted to impose highly constrained multiaxial deformation conditions, providing further insight into the material response under complex loading paths.

The combined experimental programme covering tensile, shear, notched, and punch loading conditions provides a comprehensive basis for material model calibration and validation. The numerical predictions obtained from the IGA framework are systematically compared against conventional finite element (FE) simulations and experimental results in terms of stress–strain response, deformation patterns, and failure behaviour.

Fig. 3.3 illustrates the geometries and configurations of the coupon-level specimens used in the study.

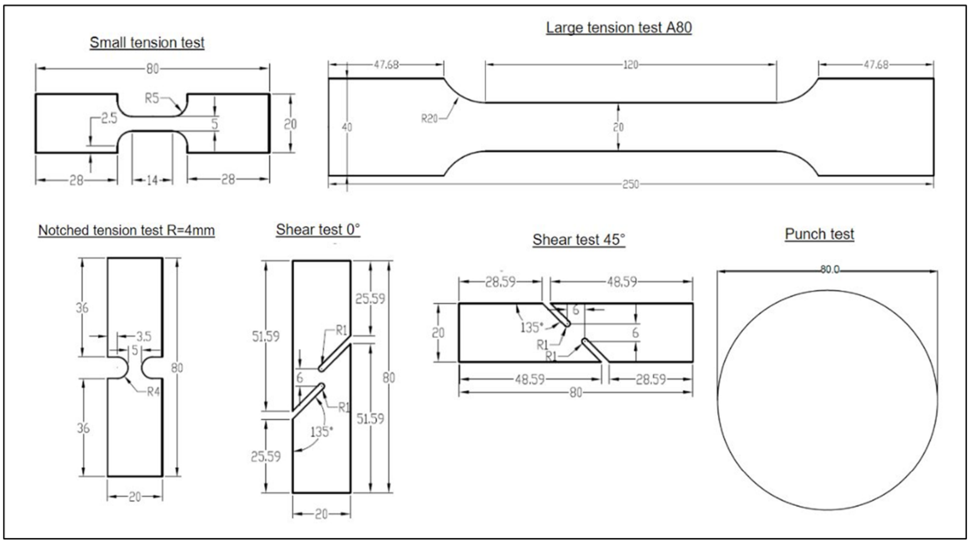

Figure 3.3: Coupon test specimens used for material characterisation and fracture calibration

The FE results serve as a benchmark for evaluating the performance of the IGA formulation, while the experimental data provide the reference for physical accuracy. Deviations between IGA and FE predictions are analysed to assess the influence of geometric representation and numerical formulation on stress localisation, strain distribution, and fracture initiation. This multi-level correlation ensures that the material and damage modelling framework accurately captures the mechanical response of 6005A-T6 and enables reliable prediction of deformation and failure behaviour within the IGA framework.

3.2.2 Component-Level Validation

At the component level, intermediate validation was conducted using representative aluminium extrusion geometries subjected to crash-relevant loading conditions. The validation was based on experimental and numerical results reported in a previous master's thesis [31], which served as a reference for assessing the predictive capability of the IGA framework. The comparison focused on deformation behaviour, stress distribution, and damage initiation under realistic boundary conditions and loading scenarios.

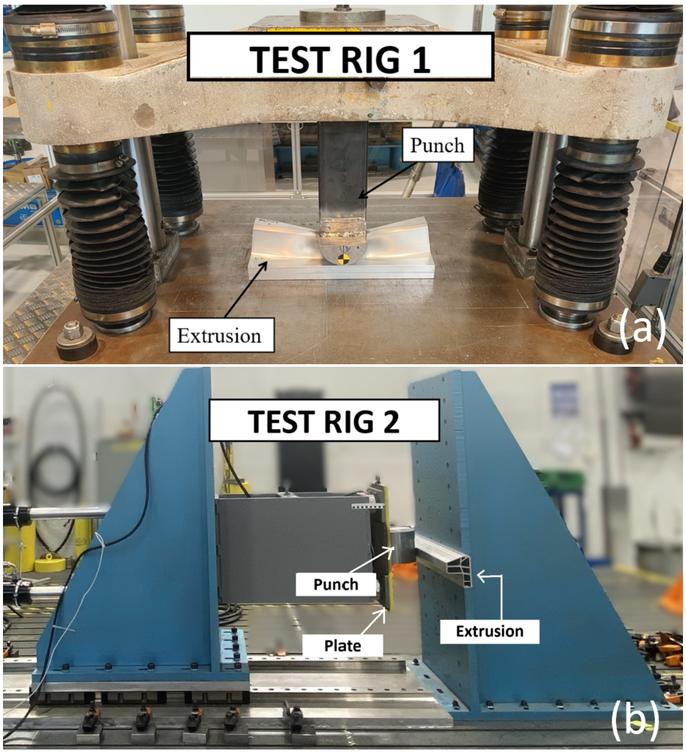

Figure 3.4: Component-level test setups for lateral crushing of extrusions: (a) test rig with a small impactor, and (b) test rig with a large impactor

To investigate the sensitivity of the model to localised deformation and contact conditions, two loading scenarios were considered for a 350 mm long extruded component. These consisted of compressive tests using impactors of different sizes, as illustrated in Fig. 3.4. A large impactor, characterised by a punch diameter of 254 mm, was used to apply a distributed load over a wider contact area, resulting in a predominantly global deformation mode. This configuration enables evaluation of the model's capability to capture overall stiffness and large-scale structural behaviour.

In contrast, a small impactor with a punch diameter of 100 mm was used to introduce highly localised loading conditions, leading to significant stress concentration and local plastic deformation. This setup is intended to assess the capability of the IGA framework to predict strain localisation and damage initiation under concentrated loading.

The numerical results obtained from the IGA simulations were compared with both conventional finite element simulations and previously conducted experimental results. The comparison was carried out in terms of force–displacement response, deformation patterns, and failure characteristics.

Fig. 3.5 illustrates the IGA-based component model employed in the validation.

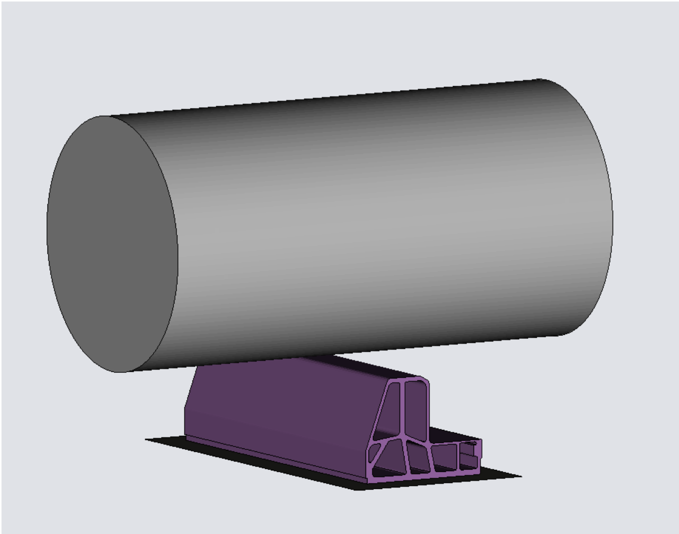

Figure 3.5: IGA-based component model used for intermediate validation

3.2.3 Assembly-Level Validation

Assembly-level validation was performed within the methodological framework to assess the applicability and robustness of the IGA formulation under realistic structural and system-level loading conditions. The validation strategy was designed to progressively increase model complexity, transitioning from a component-level model in Section 3.2.2 to an assembly-level crash configuration. In this stage, the previously defined component was integrated into a larger structural system, thereby introducing additional modelling features such as contact interactions, weld representations, and structural bosses.

The primary validation case consisted of an extrusion assembly fracture test. The corresponding numerical model included large plastic deformations, progressive damage evolution, structural connections, and detailed contact definitions. This setup was used to evaluate the capability of the IGA framework to capture fracture initiation and subsequent crack propagation within an assembled structural system subjected to highly nonlinear loading conditions.

Within this framework, the structural response was considered with respect to the coupled effects of contact nonlinearity, material degradation, and large-deformation kinematics. This was used to assess of the numerical stability and robustness of the IGA implementation in an assembly environment where multiple nonlinear mechanisms interact simultaneously.

As a second step in the assembly-level methodology, a full vehicle crash model subjected to a high-speed impact scenario was considered. In this model, the spring tower both left and right side was discretised using the IGA formulation and embedded into a conventional FE vehicle model. This hybrid modelling approach enabled a subsystem-level assessment of the IGA formulation under boundary conditions governed by global vehicle dynamics. The spring tower model was used as a secondary validation case to evaluate the transferability of the IGA approach to localised structural regions within a full-scale crash simulation.

Overall, the assembly-level validation methodology provides a hierarchical framework for assessing the IGA formulation, covering both component-scale fracture behaviour and full vehicle crash response. This ensures that the method is evaluated under both isolated and system-level conditions, including multi-body interaction, impact loading, and strongly nonlinear material behaviour.

3.3 IGA Sensitivity Analysis Methodology

A systematic sensitivity study was performed to assess the robustness, numerical stability, and computational efficiency of the IGA framework. The investigation focused on key numerical and discretization parameters that influence both solution accuracy and computational performance. In particular, the effects of strain formulation, geometric refinement, and numerical integration were evaluated under controlled variations.

3.3.1 Lumped Assumed Strain (LAS) formulation

The Lumped Assumed Strain (LAS) technique was employed to alleviate locking phenomena commonly observed in lower-order or highly constrained discretizations. Its influence on displacement accuracy, stress recovery, and overall convergence behaviour was systematically examined. Comparisons were made between standard IGA formulations and LAS-enhanced implementations to quantify improvements in numerical robustness.

3.3.2 NURBS refinement sensitivity

The effect of geometric discretization was investigated through variations in Non-Uniform Rational B-Splines (NURBS) control point spacing, specifically at 0.5 mm, 1 mm, 2 mm, and 3 mm resolutions. This study enabled the assessment of convergence characteristics with respect to mesh density, as well as the sensitivity of stress localization and deformation gradients to geometric refinement. The results provide insight into the minimum discretization level required to achieve mesh-independent solutions.

3.3.3 Computational cost and efficiency

The computational performance of each refinement level and formulation was evaluated in terms of total solution time, including assembly and solver stages. This analysis highlights the trade-off between numerical accuracy and computational expense, which is particularly relevant for large-scale simulations in engineering applications. The scaling behaviour of the IGA framework with increasing control point density was also examined.

Overall, the sensitivity study methodology provides a systematic framework for evaluating the influence of discretization parameters and numerical formulations on the accuracy, stability, and computational efficiency of the IGA framework. The outcomes of this investigation support the identification of suitable modelling parameters for subsequent simulations and validation studies.

3.4 Material Modelling and Failure Criteria

The material behaviour was modelled using an isotropic constitutive formulation combined with a stress-state-dependent failure criterion. In contrast to more advanced damage models such as the Generalized Incremental Stress State dependent damage model (GISSMO), which explicitly accounts for damage evolution under varying stress triaxiality conditions, the present study adopts a Cockcroft–Latham based failure approach to capture ductile fracture initiation.

The Cockcroft–Latham criterion provides a stress-invariant formulation for predicting the onset of damage in ductile materials and has been widely applied in metallic fracture modelling. As reported in previous work at VCC [25], more advanced models such as GISSMO offer improved predictive capability under complex loading paths. However, in the present work, the simpler isotropic damage formulation was selected to balance computational efficiency, numerical robustness, and modelling complexity, while still capturing the essential fracture behaviour of the investigated aluminium alloys.

Experimental observations indicate that the investigated extruded aluminium alloys exhibit pronounced anisotropic behaviour, which is not explicitly represented within the isotropic material model adopted in this study. The anisotropic response was characterised through directional mechanical testing, microstructural alignment analysis, and fracture surface evaluation. The extrusion process promotes the development of crystallographic texture and alignment of intermetallic particles, resulting in direction-dependent mechanical and fracture properties.

The influence of stress triaxiality on damage evolution and fracture initiation was assessed under different loading conditions. Post-failure fracture surfaces were analysed to identify the dominant ductile failure mechanisms, including void nucleation, growth, and coalescence.

Due to constraints in time and scope, fracture surface characterisation was limited to qualitative analysis using optical microscopy. This approach enabled a macroscopic assessment of fracture morphology and identification of characteristic ductile fracture features without the use of advanced surface characterisation techniques such as scanning electron microscopy. The observed fracture features were subsequently used to support the interpretation of anisotropic damage behaviour under varying loading conditions.

4

Results and Discussion

The following section presents and discusses the results obtained from the assessment of the IGA-based solid model under various loading conditions and different complexity of the model. The study evaluates the structural response, deformation behaviour, stress distribution, and triaxiality with a particular focus on the accuracy and numerical stability of the IGA formulation. The results obtained are compared with reference simulations and available experimental observations to assess the predictive capability of the developed model. For confidentiality reasons, the y-axis values in the figures have been removed.

4.1 IGA Validation Results

The comparative assessment of the IGA simulation results is conducted across multiple hierarchical levels, including the coupon, component, and assembly scales. This framework enables systematic validation of the numerical model through comparison with both experimental test data and conventional FEA results, spanning from fundamental material response to full structural behaviour. For the present study, isotropic material models are adopted throughout, assuming uniform mechanical properties in all directions, which provides a consistent baseline for evaluating the performance of the IGA framework across the different scales.

4.1.1 Coupon-Level Validation

The coupon-level results are presented to evaluate the predictive capability of the calibrated IGA framework using the experimental programme defined in the methodology. The assessment covers six representative coupon configurations, including standard tensile, large tensile, 45° shear, 90° shear, notched, and punch specimens, enabling a comprehensive evaluation of material behaviour under different stress states (Fig. 4.1).

To ensure a consistent comparison, identical geometries, boundary conditions, loading configurations, and material parameters were employed in both the IGA and conventional FE models. The IGA models were discretised using a NURBS control point

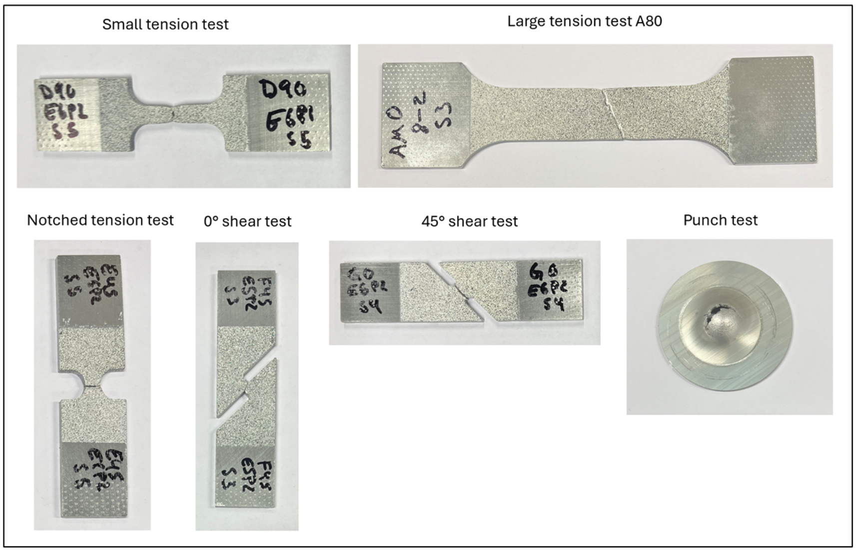

Figure 4.1: Failure patterns of the six different tested specimens.

spacing of 0.5 mm, while the corresponding FE models utilised an element size of 0.5 mm. This relatively fine discretisation was selected to minimise mesh-dependent effects and ensure that the observed differences in the results primarily reflect the performance of the constitutive and numerical formulations.

The results obtained from the coupon tests were systematically compared with conventional FEA, the IGA Box implementation, and the IGA ANSA-based modelling approach for all six coupon configurations, enabling a comprehensive assessment of the predictive capability and consistency of the different modelling strategies.

Tensile

The results demonstrate that the IGA model accurately captures the elastic–plastic behaviour of the material. The predicted stress–strain response closely follows the experimental curves and remains consistent with conventional FE predictions (Fig. 4.2), for both standard and large tensile configurations. The standard tensile specimen serves as a baseline for evaluating the material behaviour under uniaxial loading, while the large tensile specimens further highlight the model's ability to capture strain localisation and size-dependent deformation effects. This confirms the robustness and predictive capability of the IGA formulation in accurately representing both uniform and non-uniform deformation responses.

The force–displacement response further supports the observed agreement with experimental measurements for both coupon geometries. The IGA model reproduces the initial stiffness, yielding behaviour, and overall deformation response with high accuracy. In comparison, conventional FE results show slightly larger deviations in the nonlinear regime at higher strain levels. The larger tensile coupon highlights the robustness of the IGA formulation under increased deformation, indicating its suitability for modelling ductile behaviour in extruded aluminium structures.

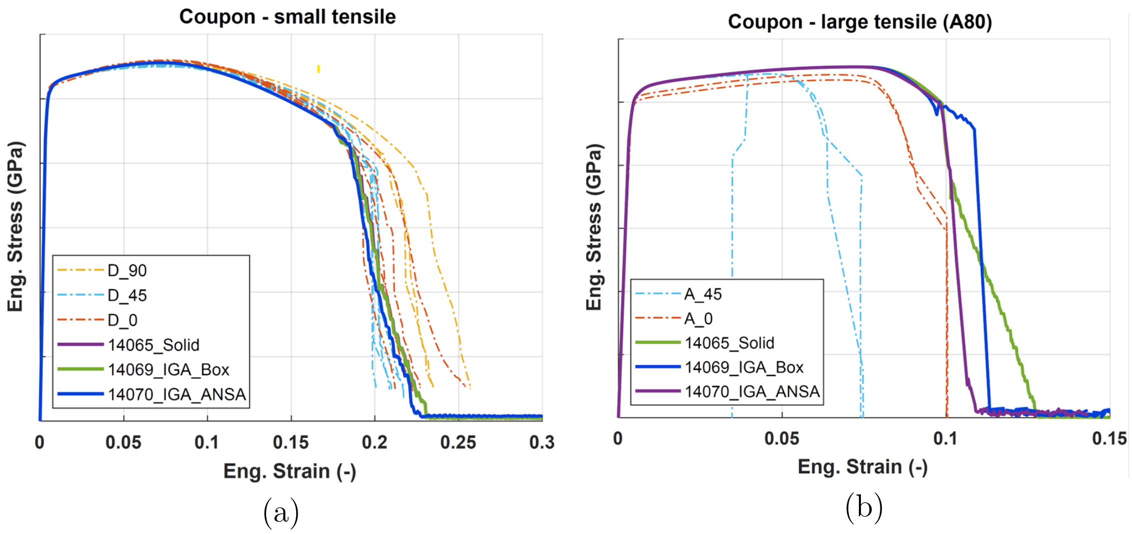

Figure 4.2: Comparison of experimental, conventional FE, and IGA simulation results for (a) standard and (b) large tensile coupon tests. Additional simulation results for different material parameter sets are provided in Appendices A–C.

Notched

The notched coupon results demonstrate the capability of the model to accurately capture stress concentration effects and strain localisation near geometric discontinuities. Consistent with the tensile cases, the IGA formulation closely follows the experimental response, indicating its ability to reliably represent the underlying material behaviour across different loading conditions.

The IGA predictions are consistent with the experimentally observed failure initiation trends, particularly in regions of peak stress. In comparison, conventional FE results exhibit greater sensitivity to mesh refinement, leading to increased variability in the predicted localisation zone. This highlights the advantage of the IGA formulation in providing a more stable and consistent representation of local deformation under high stress gradients.

Although slight variations in the predicted response are observed among the experimental, FE, and IGA results, the overall trends and failure characteristics are captured with good correlation (Fig. 4.3), despite differences in modelling approaches. Minor discrepancies are also observed between the IGA Box and ANSA-based models, which can be attributed to differences in discretisation strategies and geometric representation, leading to slight variations in local stress evaluation.

Furthermore, the higher-order continuity of NURBS basis functions contributes to a smoother stress distribution, reducing numerical artefacts commonly observed in standard finite element formulations. As a result, the IGA framework offers enhanced robustness in predicting failure initiation and localisation in regions dominated by complex stress states.

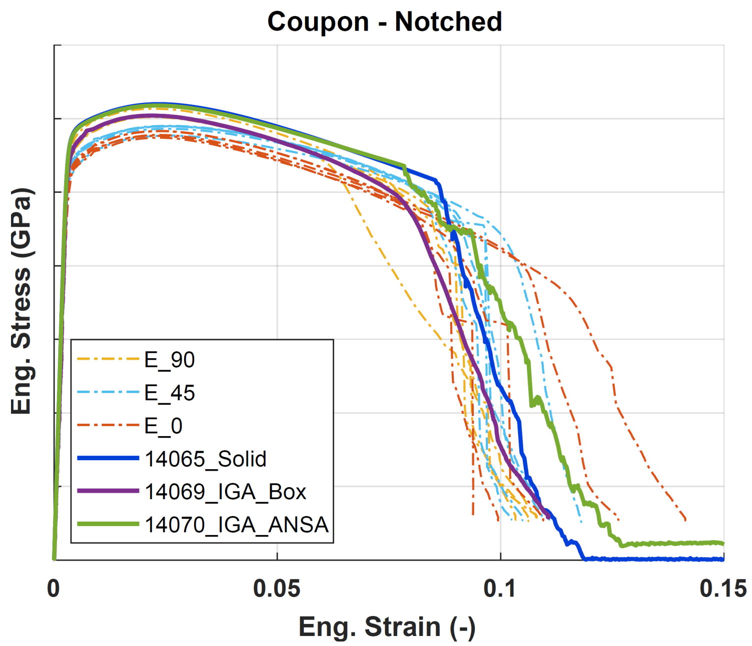

Figure 4.3: Comparison of experimental, conventional FE, and IGA simulation results for notched tensile coupon tests.

Shear

For shear-dominated loading, the 0° and 45° configurations represent mixed-mode and near-pure shear conditions, respectively. The results show that the IGA formulation accurately captures the overall deformation behaviour, with improved smoothness in the stress distribution compared to conventional FE simulations, particularly in regions with high strain gradients (Fig. 4.4).

Some discrepancies in the force response were observed for both the Shear_00 and Shear_45 cases relative to the experimental and FE results. These differences are partly due to solver limitations and differences in section force evaluation between FEA and IGA under shear-dominated, biaxial loading.

In FEA, section forces are computed element-wise with C^0 continuity, leading to stress discontinuities, while IGA provides smoother stress fields due to higher-order continuity. This results in slight variations in stress integration and force prediction.

Nevertheless, the overall shape and trend of the force–displacement curves are accurately captured and reflect the experimental observations.

The results further indicate that the IGA framework can reliably capture the dominant deformation mechanisms under different shear loading orientations, including strain redistribution and localisation effects. The 45° configuration, in particular, highlights the ability of the formulation to represent near-pure shear behaviour with consistent accuracy.

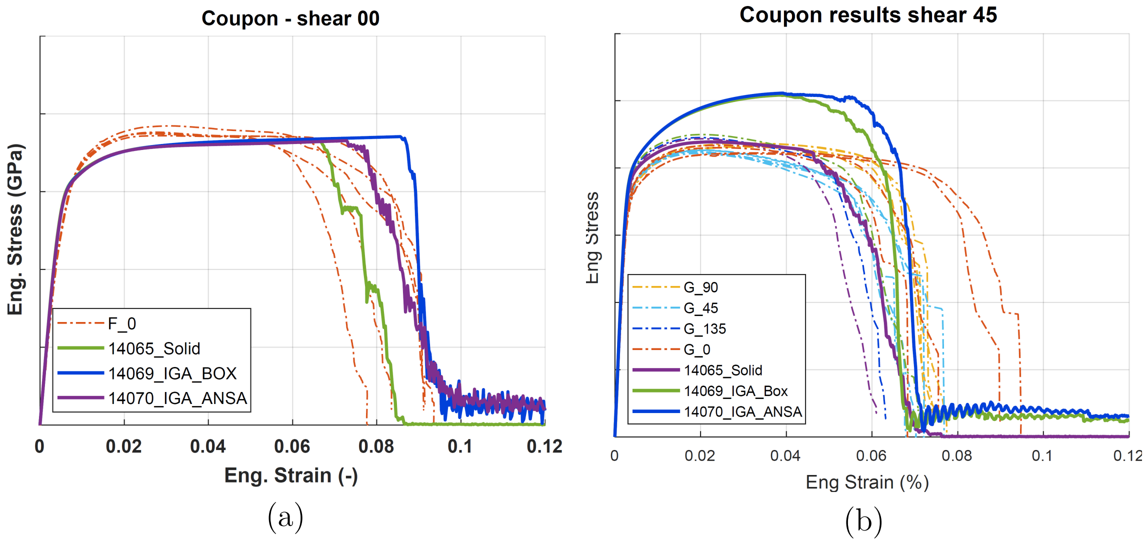

Figure 4.4: Comparison of experimental, conventional FE, and IGA simulation results for (a) 0° (mixed-mode) and (b) 45° (near-pure shear) coupon tests.

Punch

The punch test results demonstrate the robustness of the model under highly constrained, multi-axial deformation. The IGA formulation successfully reproduces both the global force–displacement response and the experimentally observed deformation patterns, confirming its applicability to complex loading scenarios (Fig. 4.5). Some discrepancies are evident in the local response, primarily due to the sensitivity of the contact interaction to the NURBS parameterisation and discretisation strategy.

This highlights a limitation of the current IGA formulation, where local response accuracy is sensitive to control point distribution and contact definition.

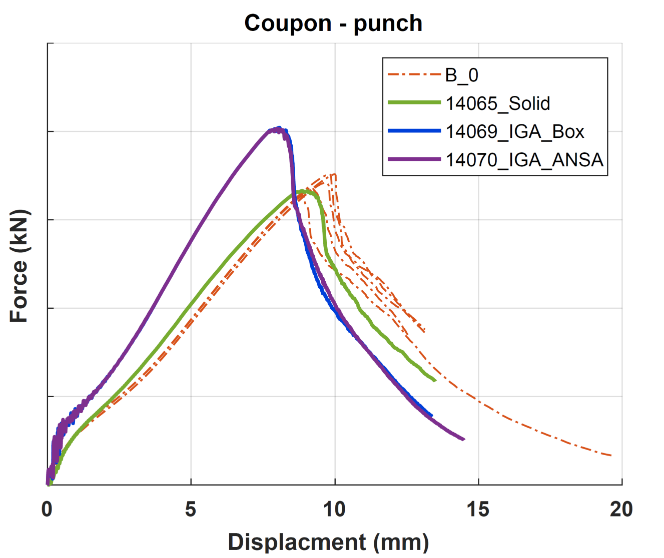

Figure 4.5: Comparison of experimental, FE, and IGA results for punch test coupons.

Overall, the comparison between IGA, FE and experimental results shows that the IGA framework provides improved numerical smoothness and stable strain localisation behaviour, while maintaining strong correlation with both benchmark simulations and physical test data. The higher-order continuity inherent to the IGA formulation contributes to more consistent stress fields and enhanced fracture prediction capability across all six coupon configurations.

A key conclusion from these results is that the IGA formulation does not require separate material model calibration to accurately reproduce the observed response, unlike cases where significant discrepancies between numerical and experimental results necessitate parameter adjustment.

These findings directly support the research objective by demonstrating that the IGA framework can reliably reproduce experimentally observed material behaviour across different stress states without requiring additional calibration. Moreover, the results indicate that the inherent smoothness of the IGA formulation enhances numerical stability under complex loading conditions. This further underscores its potential for robust and transferable application in large-scale structural simulations.

4.1.2 Component-Level Validation

The component-level assessment evaluates the structural response of aluminium extrusions under impact loading, focusing on global stiffness, deformation behaviour, and localised failure initiation. Validation is performed through comparison with experimental reference data and conventional FE results reported in a previous master's thesis. Both small and large impactor configurations are considered to represent different loading severities and deformation modes. Compared with coupon-level analyses, the component level introduces additional complexity due to combined stress states, nonlinear strain paths, and contact interactions.

4.1.2.1 Deformation Response

The deformation response is strongly influenced by the impactor size. The large impactor case exhibits a predominantly global deformation mode with smooth load transfer across the structure. The IGA predictions are consistent with the experimental observations in terms of overall stiffness, deformation patterns, and progressive collapse behaviour, while maintaining a stable numerical response.

In contrast, the small impactor case produces highly localised deformation accompanied by pronounced stress concentrations. The IGA model accurately reproduces the experimentally observed localisation behaviour and remains numerically stable in regions of high strain gradients. Compared to the large impactor configuration, the response is characterised by a more confined plastic zone and an earlier onset of local damage, reflecting the increased sensitivity of the structure to localised loading conditions.

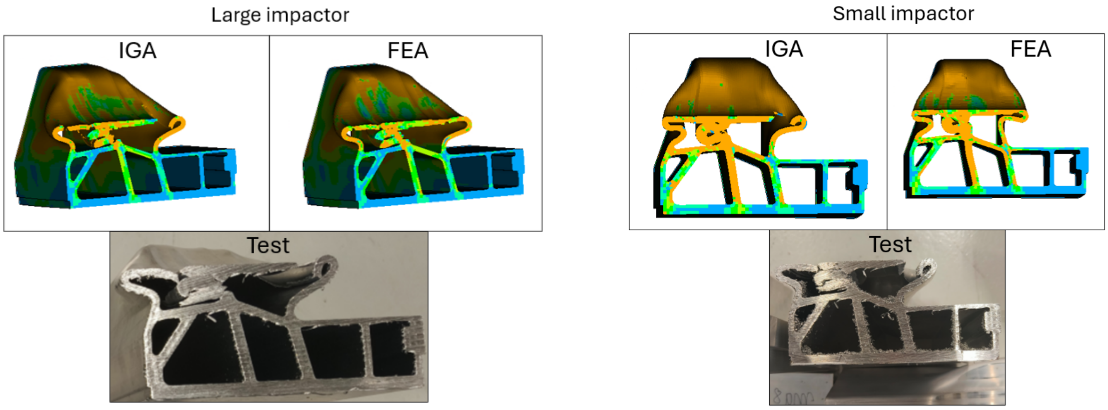

(a) (b)

Figure 4.6: Cross-sectional comparison of deformation responses for (a) the large impactor case and (b) the small impactor case.

4.1.2.2 Force–Displacement Response

The force–displacement response shows strong agreement between the IGA simulations and the experimental data for both loading cases. The large impactor configuration exhibits a smooth response with accurate prediction of the global structural stiffness and energy absorption characteristics. The response follows the experimental trend throughout the loading history, demonstrating the ability of the IGA formulation to capture the overall load-carrying behaviour of the structure.

For the small impactor case, the force–displacement response exhibits a steeper initial gradient and a more pronounced reduction in stiffness following yielding, reflecting the highly localised nature of the deformation. Despite the increased complexity associated with stress concentrations and local plasticity, the IGA model accurately reproduces the overall shape and magnitude of the experimental response.

Compared with the conventional FE results, the IGA formulation demonstrates improved consistency, particularly in the post-yield regime where a smoother and more stable response is observed. This behaviour highlights the capability of the IGA approach to represent both global and local deformation mechanisms within a unified framework.

Overall, the component-level results indicate a strong correlation between the IGA predictions and experimental observations across both loading scenarios. The formulation successfully captures the global structural response, localised deformation behaviour, and post-yield characteristics of the aluminium extrusion components. These findings demonstrate the robustness and predictive capability of the IGA formulation, confirming its ability to accurately represent both global and local deformation mechanisms and supporting its application in component-level crashworthiness simulations in line with the research objectives.

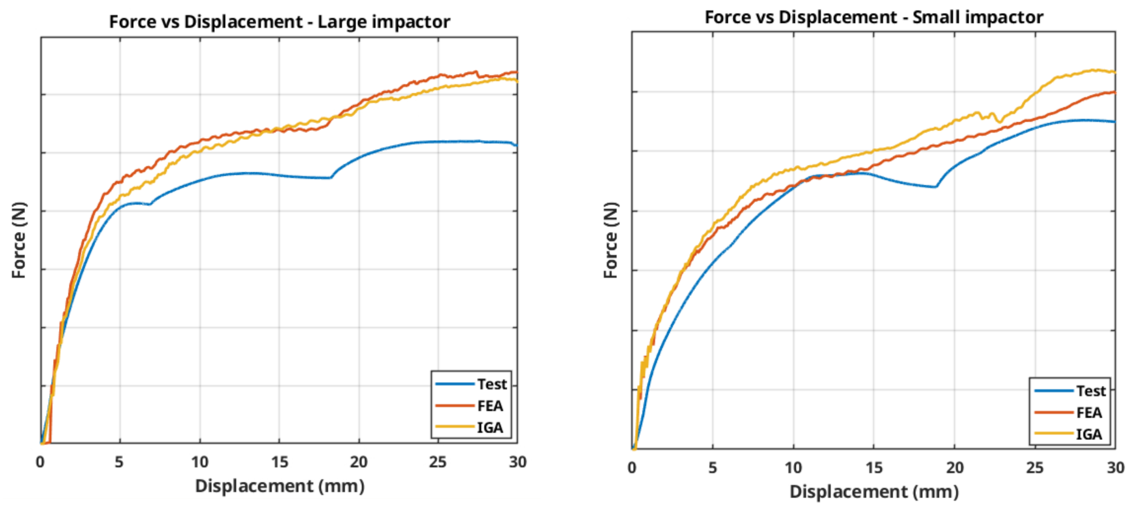

(a) (b)

Figure 4.7: Comparison of experimental, FE, and IGA force–displacement responses for (a) the large impactor case and (b) the small impactor case.

4.1.3 Assembly-Level Validation

The extrusion assembly model was used to evaluate the capability of the IGA formulation to predict deformation behaviour, fracture initiation, and structural response at the assembly level.

The force–displacement response obtained from the IGA simulation closely follows the experimental data. Some variation in the peak force is observed, with the IGA predictions showing a closer match to the experimental results, while the conventional FE model tends to underestimate the peak force (Fig. 4.8). These differences are further examined in the sensitivity analysis.

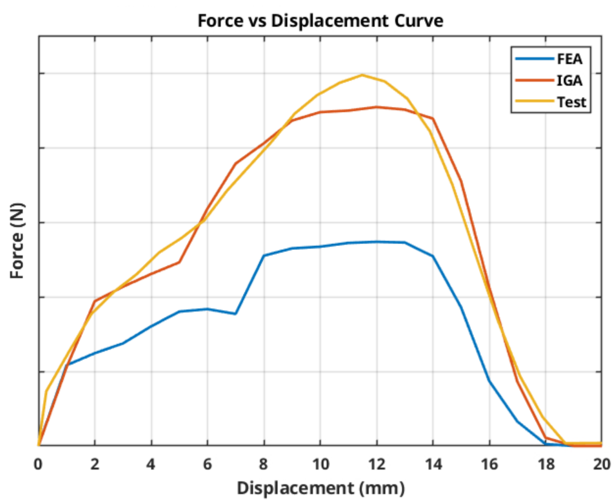

Figure 4.8: Force–displacement response for the extrusion assembly fracture test comparing experimental, FE, and IGA results.

Overall, the global stiffness, peak force, and post-peak softening behaviour are captured with satisfactory accuracy, demonstrating the capability of the IGA framework to effectively represent both the structural response and the subsequent damage evolution.

In addition, the IGA formulation provides a smoother representation of the deformation and stress fields due to the higher continuity of the spline-based basis functions. The model maintains stable numerical behaviour throughout the simulation, including during damage initiation and propagation, where conventional FE approaches are often more sensitive to mesh dependency.

Furthermore, the comparison of extrusion crash test results with conventional FEA and IGA predictions indicates consistent representation of the failure section geometry and local deformation characteristics. The observed failure regions and deformation patterns in the critical section are well captured across all approaches (see Fig. 4.9), supporting the validity of the IGA model at the assembly level. In addition, the IGA model captures the fracture initiation point with greater precision, showing an improved correlation with the experimental observations.

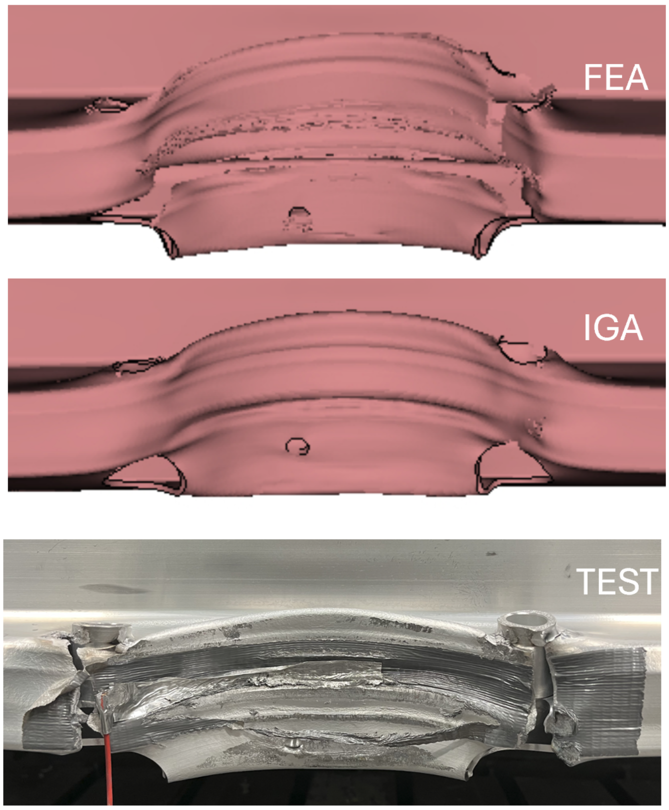

Figure 4.9: Comparison of extrusion crash test results with FEA and IGA predictions at assembly level.

4.1.3.1 Full-Vehicle Crash Validation

To investigate the applicability of IGA in a realistic crash environment, a full-vehicle assembly model was analysed, in which the spring tower region was represented using IGA and coupled to the surrounding structure through a hybrid FE–IGA approach. The study demonstrated that IGA simulations can be successfully executed within a full-car model, enabling selective replacement of critical structural regions with IGA while maintaining compatibility with conventional finite element formulations.

However, due to time constraints, the results of the full-vehicle IGA simulation could not be fully validated against experimental or reference data. Despite this limitation, the study highlights the capability of the IGA framework to operate in a hybrid modelling environment, offering the potential for improved computational efficiency and solution accuracy.

Overall, these findings fulfil one of the key objectives of the thesis by demonstrating that IGA can be integrated into large-scale industrial applications, allowing complex regions such as the spring tower to be modelled with higher fidelity while the remaining structure is retained using standard FE discretisation.

4.2 IGA Sensitivity Analysis Results

Sensitivity analysis was conducted to evaluate the influence of numerical formulations and discretization parameters on the structural response, convergence behaviour, and computational efficiency of the IGA framework. The results obtained provide insight into the robustness of the implemented formulations and support the selection of suitable modelling parameters for subsequent simulations. In particular, the influence of NURBS refinement, integration schemes, control point distribution, and additional parameters was systematically examined to identify their effects on solution accuracy and numerical stability. The analysis further highlights the role of these parameters in achieving reliable predictions for large-scale applications. These findings serve as a guideline for optimising the IGA setup to ensure accurate and efficient simulation performance.

4.2.1 Lumped Assumed Strain (LAS) Formulation

The IGA solid formulation implemented in LS-DYNA is based on NURBS basis functions, which provide exact geometric representation and higher-order continuity of the displacement field. While these properties improve geometric fidelity and solution smoothness, the increased continuity may also introduce volumetric locking effects under near-incompressible deformation conditions.

To mitigate this issue, the LAS formulation was employed within the `*IGA_SOLID` definition. The LAS approach improves numerical stability by projecting the strain field into a reduced strain representation, thereby reducing excessive stiffness caused by locking phenomena. In this study, the LAS formulation was activated using **LAS = 1**, as shown below:

```
*IGA_SOLID
$#   sid     pid    nisr    niss    nist     rid      lcs      las
       3       3     0.      0.      0.       3                  1
```

The comparison presented in Fig. 4.10 illustrates the influence of the LAS formulation on the deformation behaviour of the IGA solid model. Without LAS activation, the structure exhibited noticeable locking behaviour and artificially stiff deformation patterns. In contrast, the LAS-enhanced formulation showed a smoother deformation response and improved flexibility, indicating a reduction in volumetric locking effects. The LAS formulation significantly improves the robustness, numerical stability, and physical consistency of the IGA solid simulations under nonlinear loading conditions. This directly supports the research objective by demonstrating that the IGA formulation can effectively mitigate volumetric locking issues that commonly affect conventional FEM formulations.

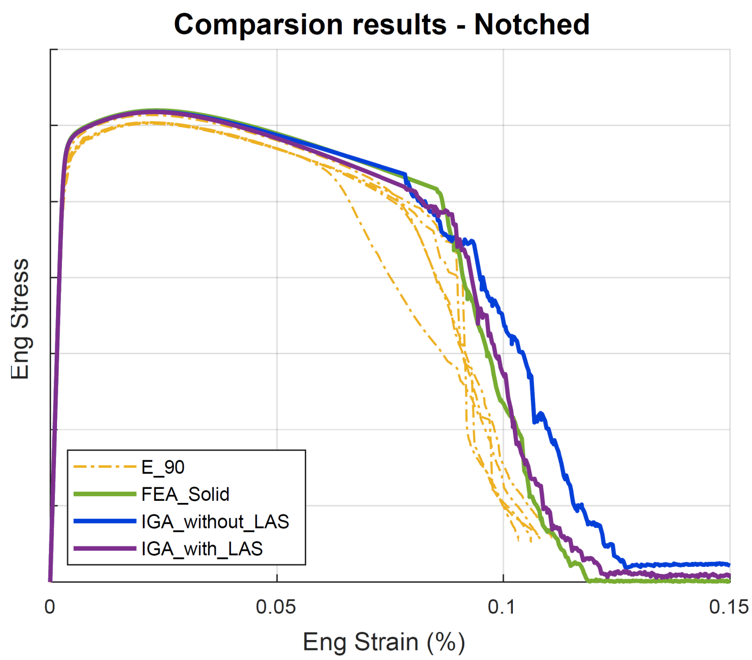

Figure 4.10: Comparison of IGA solid response without and with LAS formulation, highlighting the reduction of volumetric locking effects.

4.2.2 Effect of NURBS Refinement

The sensitivity study on NURBS refinement revealed a clear dependency between control point spacing and solution accuracy as shown in Fig. 4.11. Coarse discretizations with 4 mm and 3 mm spacing produced acceptable global deformation behaviour; however, localized stress concentrations and deformation gradients were less accurately captured. Refinement to 2 mm resulted in improved stress distribution and more stable deformation patterns.

The finest discretization of 1 mm and 0.5 mm demonstrated the highest level of accuracy and provided mesh-independent behaviour in the investigated loading conditions. In particular, strain localisation and geometric deformation were captured more consistently with the refined control point distribution. However, the improvement in accuracy between the 2 mm and 1 mm models was relatively limited.

However, the 2 mm NURBS discretisation exhibited discontinuities in the predicted response and reduced numerical stability compared to the finer models. Although the simulations could be completed by reducing the number of CPUs, the occurrence of LS-DYNA Error 50179 during parallel execution indicated limitations associated with the current solver implementation. This issue is further discussed in Chapter 5.

A key limitation identified in this study is the sensitivity of the IGA formulation to solver stability issues under parallel execution for coarser meshes, which affects the consistency and reliability of the results.

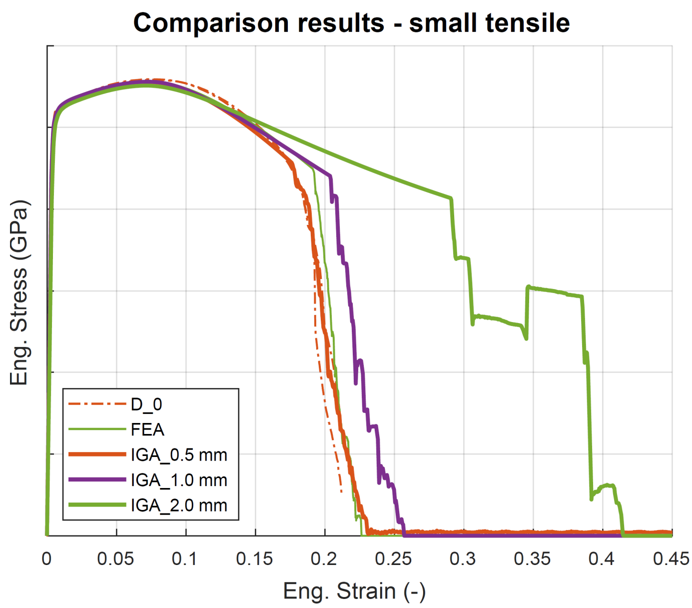

Figure 4.11: Effect of NURBS control point refinement on deformation and stress distribution.

These observations confirm the strong influence of discretisation on the accuracy and robustness of the IGA formulation. The results support the research objective by showing that IGA can achieve mesh-independent and physically consistent solutions with fewer degrees of freedom compared to conventional FE approaches when an appropriate refinement level is used.

4.2.3 Computational Performance Evaluation

The computational efficiency of the proposed IGA framework was assessed by comparing its performance with conventional FEM in terms of degrees of freedom (DOFs), convergence behaviour, and computational cost.

Additionally, smoother stress distributions were obtained without requiring extensive post-processing procedures. Although the assembly procedure of IGA may involve slightly higher computational complexity per element, the improved convergence characteristics compensated for this increase, resulting in efficient overall performance.

The results confirm that the IGA formulation provides an efficient and accurate alternative to conventional FEM. This finding directly addresses the research objective by demonstrating that improved accuracy and smoother convergence can be achieved with reduced computational effort.

Table 4.1: Efficiency comparison between FEM and IGA extrusion crash assembly

Method	**CPUs**	**CPU Time** (s)	**Max Stress** (MPa)	**Displacement** (mm)
FEM – Fine (1 mm)	200	19368	297.2	77.1
IGA – Fine (1.5 mm)	200	13499	311.65	79.2
IGA – Fine (2 mm)	200	10691	311.69	78.9
IGA – Coarse (3 mm)	200	8778	311.71	77.2

The comparison indicates that the IGA model achieved lower error values with significantly fewer DOFs compared to FEA. Furthermore, the computational time required for the converged IGA solution was substantially lower than that of the refined FEM model.

The smoother convergence trend observed in the IGA formulation highlights the superior approximation capability of NURBS-based basis functions for structural analysis applications.

The convergence study compares the performance of conventional FEA and IGA using an identical extrusion assembly model. The results demonstrate that the IGA formulation exhibits smooth and consistent convergence behaviour, whereas the FEA model experiences convergence difficulties associated with numerical instabilities (Fig. 4.12). These issues, observed in the FEA-based model, are currently under investigation by the Volvo team to gain further understanding. Such instabilities adversely affect the convergence characteristics of the conventional FE approach.

Furthermore, the IGA model achieved a higher level of accuracy with substantially fewer degrees of freedom (DOFs) than the corresponding FEM discretisations. Accurate and converged solutions were obtained with lower computational effort compared to highly refined FE models. This behaviour highlights the superior approximation properties of NURBS-based basis functions, which enable precise representation of the structural response while reducing discretisation requirements and improving numerical efficiency.

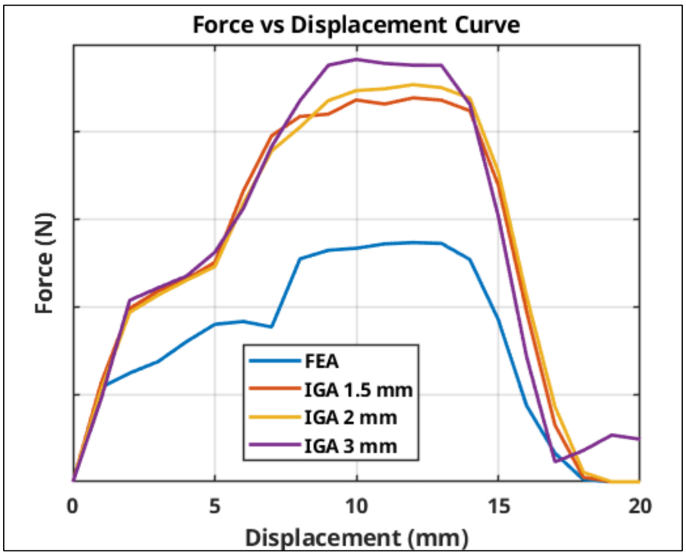

Figure 4.12: Comparison of model convergence results between FEA and IGA for an identical crash model setup.

4.3 Material Behaviour and Damage Evolution

The following sections provide material-level insights that support the interpretation of the observed mechanical behaviour and numerical simulation results.

4.3.1 GISSMO Damage Model

The GISSMO material formulation, previously calibrated for hexahedral solid elements within an earlier project at VCC [25], was utilised in the present work to model ductile damage and failure behaviour under crash loading conditions. The GISSMO model accurately reproduced the experimentally observed stress–strain response and localisation behaviour, confirming its suitability for IGA-based solid simulations.

The validation results demonstrated that the GISSMO formulation was capable of accurately capturing the stress distribution, localisation behaviour, and necking response during tensile deformation. Following the coupon-level assessment, the material model was implemented in component-level crash simulations involving thin-walled aluminium extrusion subjected to lateral crushing.

At the component level, the solid element discretisation provided a robust representation of the extrusion geometry and enabled accurate prediction of the experimentally observed buckling behaviour and overall force–displacement response. The enhanced geometric fidelity of the solid formulation allowed local deformation modes and structural instabilities to develop naturally without the need for additional geometric imperfections or numerical adjustments.

The predicted force response remained stable throughout the progressive deformation process and closely followed the experimentally observed collapse behaviour. Furthermore, the use of solid elements improved the representation of local stress states and through-thickness deformation, both of which are essential for capturing complex buckling and damage mechanisms in thin-walled extrusion structures.

4.3.2 Hardness Evolution and Heat Treatment Response

The hardness behaviour of 6005 and 6082 aluminium alloys shows a clear dependence on alloy composition and heat treatment conditions. 6082 exhibits a significant increase in hardness with increasing solution heat treatment temperature, whereas 6005 remains comparatively less sensitive to variations in solutionising temperature (Fig.4.13). This behaviour is primarily associated with the higher Mg and Si content in 6082, which promotes enhanced precipitation hardening during ageing [5].

During natural ageing, both alloys exhibit an increase in hardness; however, 6082 demonstrates a stronger dependence on prior solution heat treatment temperature. Higher solutionising temperatures increase the supersaturation of Mg and Si, thereby promoting the formation of Guinier–Preston (GP) zones and β-Mg_2Si precipitates [5]. The larger volume fraction of strengthening precipitates contributes to the superior hardening response observed in 6082.

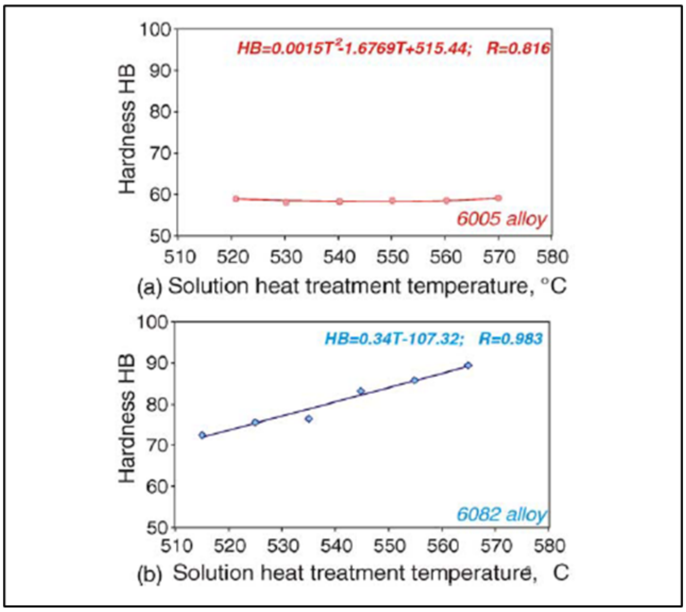

Figure 4.13: Influence of solution heat treatment temperature on hardness of: (a) 6005 alloy and (b) 6082 alloy [5], Reproduced with permission.

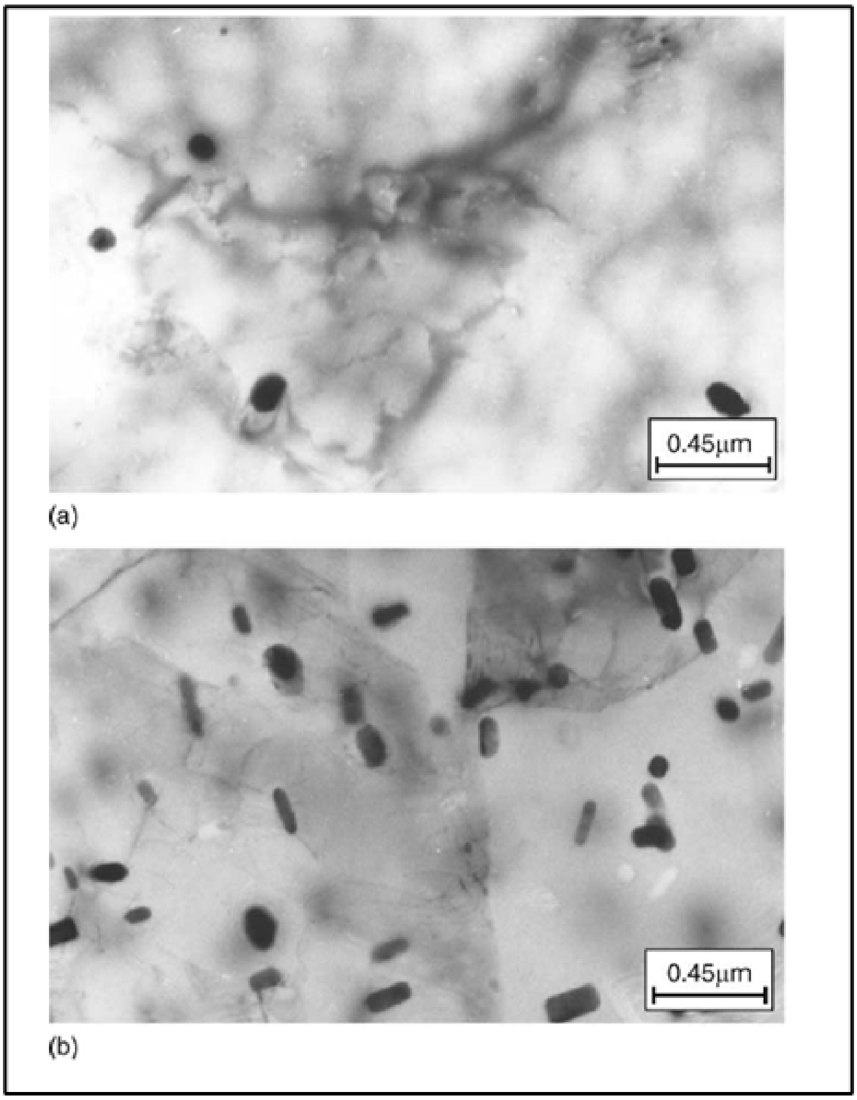

Figure 4.14: Microstructures of the 6005 and 6082 alloys after the ageing process: (a) 6005 alloy and (b) 6082 alloy [5], Reproduced with permission.

In contrast, 6005 contains a lower total alloying content, resulting in reduced precipitation strengthening capability and a comparatively lower volume fraction of strengthening phases (Fig.4.14). Consequently, the hardening response during natural ageing is less pronounced [5].

In addition, the more uniform precipitation behaviour in 6005 leads to a relatively isotropic mechanical response with improved ductility. This difference highlights the strong interaction between alloy composition, heat treatment conditions, and resulting microstructural evolution.

4.3.3 Microstructural Influence and Anisotropy

The differences in mechanical response between 6005 and 6082 are strongly related to their microstructural evolution during extrusion and heat treatment. In particular, the higher Mn content in 6082 promotes the formation of Mn-rich dispersoids, such as α-$Al_{12}(FeMn)_3Si$, during homogenisation. These dispersoids act to pin grain boundaries and inhibit recrystallisation, thereby preserving a fibrous grain structure and promoting a pronounced crystallographic texture [32, 33].

The resulting influence on plastic anisotropy is evident in Fig.4.15, which presents the evolution of the Lankford parameter (r-value) with strain for different loading directions. Consistent with the underlying microstructural differences, 6082 exhibits significantly higher and more direction-dependent r-values than 6005. This is particularly pronounced in the 45° direction, where average values reach approximately 1.73. In contrast, 6005 remains comparatively stable across all orientations, with r-values generally below 1.2. The larger spread between the 0°, 45°, and 90° directions in 6082 indicates a stronger plastic anisotropy and a greater sensitivity of deformation behaviour to loading direction.

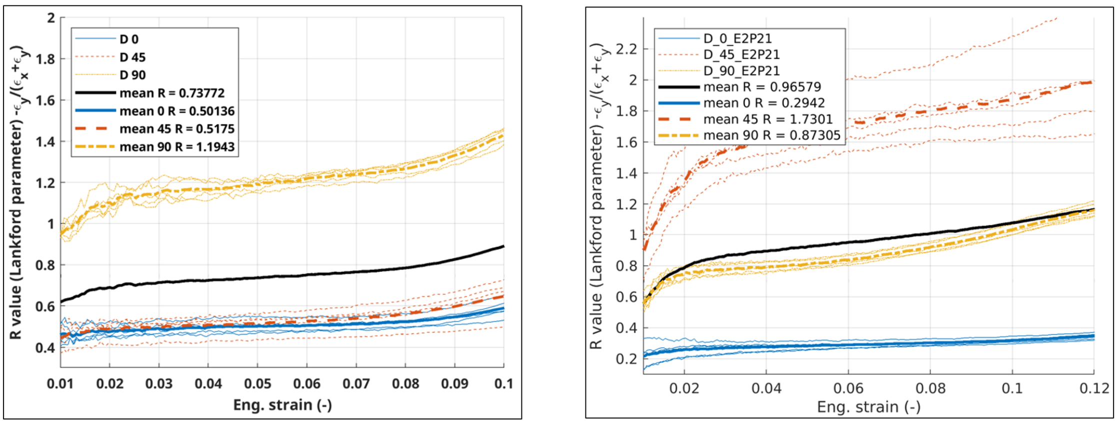

(a) (b)

Figure 4.15: Comparison of Lankford parameters (r-values) for (a) 6005A-T6 and (b)6082-T6 aluminium alloys as a function of loading direction.

The pronounced peak observed at 45° in 6082 suggests that plastic flow is strongly governed by the retained extrusion texture and elongated grain morphology. This is consistent with the suppression of recrystallisation by Mn-rich dispersoids, which stabilise deformation-induced crystallographic orientations and thereby intensify directional dependence in plastic response. In contrast, the relatively uniform r-values measured for 6005 indicate a weaker texture development and a more equiaxed grain structure, resulting in a more isotropic deformation behaviour.

Consistent with this observation, the higher mean r-values in 6082 indicate a greater resistance to thickness reduction during tensile deformation. While elevated r-values are generally beneficial for sheet metal formability, the pronounced directional variation may result in non-uniform deformation and reduced process robustness under multi-directional loading conditions. In contrast, the more uniform r-value distribution observed in 6005 reflects enhanced deformation stability, in line with its higher ductility and more homogeneous plastic response.

These differences are further reinforced by the alignment of intermetallic particles and the retained extrusion texture, both of which contribute to the pronounced anisotropic behaviour in 6082. As a result, the mechanical properties of this alloy-including strength, ductility, and formability-exhibit a strong dependence on loading orientation [34, 32].

In contrast, 6005 contains a lower density of Mn-rich dispersoids due to its reduced Mn content, which allows more complete recrystallisation during thermomechanical processing. This results in a finer, more equiaxed grain structure with reduced texture intensity, thereby promoting a more isotropic mechanical response. This behaviour aligns with the more uniform deformation characteristics discussed in the preceding section on tensile behaviour.

The higher strength observed in 6082 can therefore be attributed to the combined effects of precipitation strengthening and dispersoid strengthening. However, this strengthening mechanism also leads to reduced ductility and an increased tendency for strain localisation, reflecting a more pronounced strength–ductility trade-off relative to 6005. In comparison, 6005 exhibits improved ductility, enhanced formability, and greater tolerance to variations in processing conditions, as previously outlined in the processing behaviour section.

From a processing perspective, these microstructural differences also manifest in extrusion behaviour. 6005 demonstrates more stable material flow and a reduced susceptibility to surface defects such as tearing and flow localisation. In contrast, the higher Mn content in 6082 promotes dispersoid formation and influences recrystallisation kinetics, making the alloy more sensitive to processing parameters. Nevertheless, when optimised heat treatment and extrusion conditions are applied, 6082 is capable of achieving superior structural performance [5].

Overall, the results presented in this section highlight the direct link between microstructural state and anisotropic mechanical response. 6082 is characterised by higher strength, greater hardening potential, and pronounced anisotropy arising from its dispersoid-stabilised, texture-rich microstructure. In contrast, 6005 exhibits a more homogeneous grain structure, resulting in improved ductility, more uniform deformation behaviour, and enhanced processing robustness. These findings provide a microstructural basis for the differences in macroscopic mechanical behaviour that will be further considered in the subsequent discussion of formability and application performance.

4.3.4 Microscopic Evaluation of Fracture Surfaces

Fracture surface analysis was performed to investigate the governing failure mechanisms and to support the interpretation of the observed macroscopic mechanical behaviour of the investigated aluminium alloys. The evaluation was conducted using optical microscopic imaging, enabling detailed observation of fracture morphology, void formation, and crack propagation characteristics.

The fracture surfaces of 6005 specimens predominantly exhibit ductile fracture characteristics characterised by uniformly distributed dimple morphology. These dimples indicate that failure is governed primarily by micro-void nucleation, growth, and coalescence during plastic deformation. The comparatively homogeneous microstructure of 6005 promotes more uniform plastic flow prior to fracture, resulting in a relatively stable and less directional failure response.

In contrast, the fracture surfaces of 6082 exhibit a more heterogeneous morphology combining ductile and directional fracture features. Although dimple structures remain visible, elongated voids and aligned fracture patterns are observed along the extrusion direction. This directional behaviour is associated with aligned intermetallic particles and Mn-rich dispersoids introduced during extrusion, which act as preferential sites for local damage initiation and crack propagation.

Furthermore, localised regions exhibiting quasi-brittle characteristics are observed in 6082, particularly under higher-strength conditions. These regions are characterised by flatter fracture features and reduced evidence of plastic deformation, indicating increased strain localisation and earlier damage initiation. The alignment of particle clusters and microstructural stringers further contributes to anisotropic crack growth behaviour and heterogeneous deformation mechanisms.

The microscopic observations correlate well with the experimentally observed macroscopic response, confirming that 6082 exhibits stronger anisotropic behaviour and lower ductility compared to 6005 (Fig.4.16). Overall, the fracture surface evaluation demonstrates that microstructural alignment and particle distribution play a significant role in governing damage evolution and fracture propagation in extruded aluminium alloys.

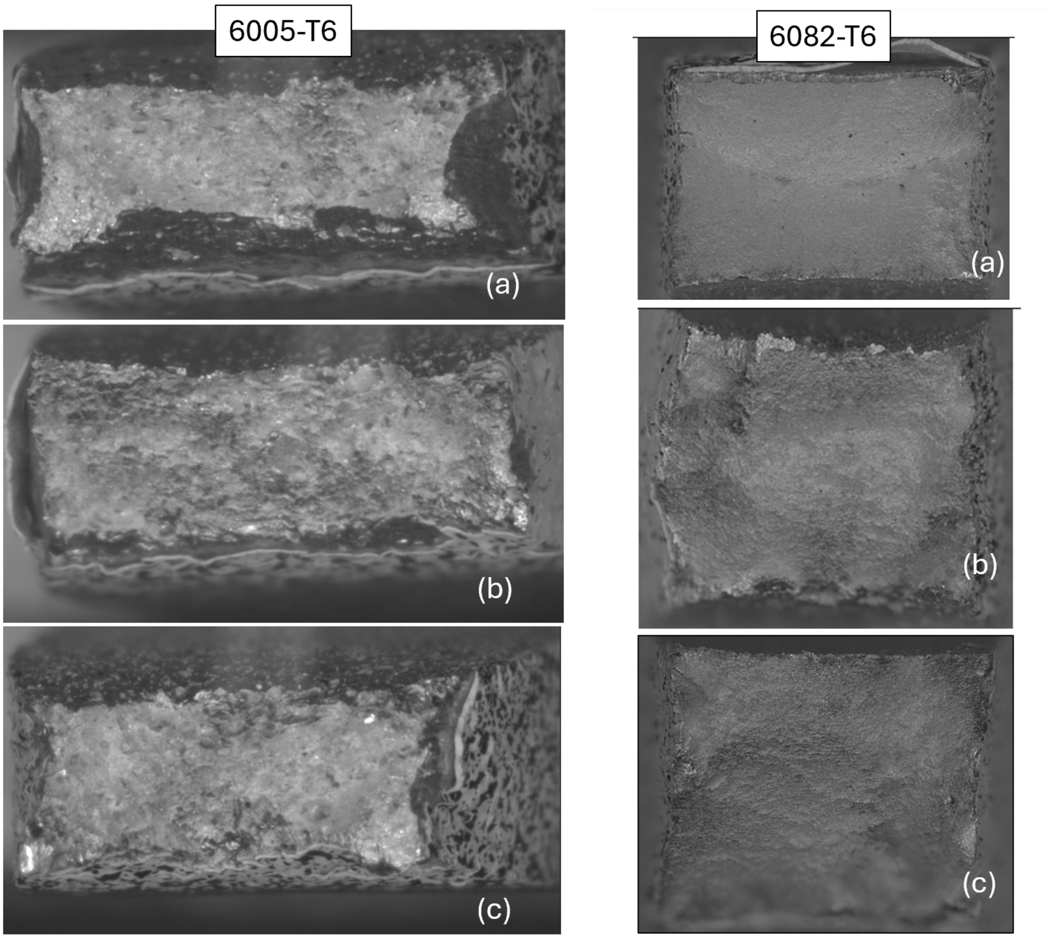

Figure 4.16: Microscopic fracture surfaces of 6005A-T6 and 6082-T6 tensile specimens, illustrating differences in fracture morphology, ductile void formation, and directional crack propagation. Images (a), (b), and (c) correspond to loading orientations of 0°, 45°, and 90° relative to the extrusion direction, respectively.

4.4 Summary of Research Findings

The key research questions defined in Chapter 1.3 are addressed based on the results obtained in this study as follows:

1. **Stress–strain prediction:** The IGA framework accurately reproduces the experimental stress–strain behaviour across all coupon tests without requiring additional calibration of material parameters (see Section 4.1.1, particularly tensile and notched results in Fig. 4.2 and Fig. 4.3).

2. **Component and assembly performance:** IGA demonstrates strong predictive capability at both component and assembly levels, accurately capturing deformation behaviour, stiffness response, and failure initiation (see Sections 4.1.2 and 4.1.3, with representative results shown in Fig. 4.6, Fig. 4.7 and Fig. 4.8).

3. **Geometric and numerical advantages:** The IGA formulation provides exact geometry representation and higher-order continuity, resulting in smoother stress fields and improved numerical stability compared to conventional FE methods (see Section 4.2. These advantages are demonstrated through the LAS formulation (Fig. 4.10), improved convergence behaviour (Fig. 4.12) and enhanced computational efficiency compared to FEM (Table 4.1).

4. **Comparison with FE methods:** Compared to traditional FEA, IGA shows improved stress distribution, smoother deformation patterns, and more stable energy absorption behaviour, particularly in nonlinear regimes (see Sections 4.1.1 and 4.1.2, with comparisons illustrated in Fig. 4.2, Fig. 4.6, and Fig. 4.12).

5. **Numerical robustness:** The IGA framework exhibits stable convergence behaviour under nonlinear dynamic loading conditions, although sensitivity to discretisation and solver limitations was observed in specific cases (see Sections 4.2.2 and 4.2.3, with key observations in Fig. 4.11 and Fig. 4.12).

6. **Industrial applicability:** The results demonstrate that IGA is sufficiently mature for integration into automotive crash simulations, particularly through hybrid FE–IGA approaches for large-scale models (see Section 4.1.3.1 and assembly-level validation in Fig. 4.9). However, challenges remain, including higher preprocessing complexity, sensitivity to discretisation parameters, and current limitations in solver robustness and modelling workflows, which may restrict its widespread industrial adoption.

7. **Effect of heat treatment:** Heat treatment significantly influence both anisotropy and mechanical properties of extruded aluminium. In 6082, higher solution heat treatment temperatures enhance precipitation hardening, resulting in increased strength and a more pronounced anisotropic response, while lower sensitivity in 6005 leads to more uniform behaviour and lower strength (see Section 4.3.2 and Fig. 4.13).

8. **Effect of alloying elements:** The alloy composition strongly influences the anisotropy, and higher levels of Mn, Mg, and Si in 6082 promote dispersoids and precipitates, leading to pronounced anisotropy with higher strength but lower ductility. In contrast, the lower alloying content in 6005 results in a more homogeneous microstructure and a more isotropic response with higher ductility (see Section 4.3.3, Fig. 4.15 and Fig. 4.16).

5

Challenges and Limitations

This chapter critically evaluates the main limitations encountered during the implementation and application of the IGA framework. While the results demonstrate its potential for crashworthiness applications, several technical and practical challenges remain, particularly regarding solver maturity, numerical implementation, preprocessing workflows, and verification.

5.1 Solver and Numerical Limitations

A key limitation is the current maturity of the IGA implementation in LS-DYNA, especially for solid formulations. The development status can be considered preliminary, leading to reduced numerical robustness compared to conventional finite element methods. Limitations in controlling advanced modelling parameters restrict flexibility, while issues related to stability, discretisation sensitivity, and parallel scalability indicate that the solver is not yet fully optimised for industrial-scale simulations.

The numerical performance is also influenced by implementation constraints. Inefficient CPU utilisation and sensitivity to NURBS parameterisation and control point spacing were observed. Additionally, the lack of well-established stabilisation techniques contributes to inconsistent solution robustness. As a result, achieving stable simulations requires careful parameter tuning, increasing model setup complexity.

5.2 Preprocessing and Modelling Challenges

The preprocessing workflow presents further challenges. Although ANSA provides a structured modelling environment, its support for IGA-specific features is not fully integrated, resulting in limited automation. Key steps such as spline definition, trimming, Part ID consistency, and connectivity verification require manual intervention, increasing both modelling time and the risk of user-induced errors.

The Box method introduces an additional limitation, as it relies on an intermediate finite element interpolation mesh for trimmed geometries. Consequently, the workflow is not fully CAD-driven and still depends on conventional meshing procedures. Maintaining consistency between the interpolation mesh, background integration mesh, and geometric representation becomes increasingly difficult for complex structures.

5.3 Verification and Practical Constraints

Another limitation is the lack of mature debugging and verification tools for IGA. Unlike conventional finite element approaches, standardised mesh quality metrics and automated validation procedures are limited. Critical aspects such as knot vector definitions, patch continuity, and geometric mapping must often be verified manually, reducing workflow efficiency and increasing the potential for errors.

Overall, while IGA offers clear advantages in geometric accuracy and solution smoothness, its industrial adoption is currently constrained by solver limitations, numerical sensitivity, and incomplete preprocessing integration. Conventional finite element methods therefore remain more robust for large-scale applications.

6

Conclusion

The present study investigated the feasibility and effectiveness of the IGA framework for structural crash and large-deformation simulations at both component and assembly levels, with a focus on numerical accuracy, robustness, and computational performance.

The results demonstrate that IGA provides a unified representation of geometry and solution fields through spline-based basis functions, leading to improved geometric fidelity and smoother stress distributions compared to conventional finite element discretisations. The higher-order continuity enhances numerical accuracy and improves correlation with experimental and reference results, particularly in capturing nonlinear deformation behaviours such as buckling, plastic hinge formation, and progressive collapse. This directly supports the research objective of improving prediction accuracy and smoothness compared to conventional FEM.

The material characterisation results confirm that the experimental stress–strain behaviour can be accurately reproduced using the IGA framework without extensive parameter recalibration, demonstrating consistency of the numerical formulation.

At the component and assembly levels, the IGA framework remained stable under complex loading conditions involving contact, large deformations, and nonlinear material behaviour. The models successfully captured global deformation patterns and key crash mechanisms. In addition, the hybrid FEA–IGA approach demonstrated the potential to improve local deformation predictions while maintaining computational efficiency for large-scale simulations. These results validate the ability of the framework to capture both global and local structural responses under crash-relevant conditions.

Comparative analyses indicate that IGA achieves similar global response predictions to conventional FEM while offering clear advantages in geometric accuracy, stress smoothness, and numerical stability. The reduction in stress oscillations and improved continuity contribute to a more consistent representation of deformation behaviour.

The sensitivity studies highlight that spline refinement, numerical integration, and strain formulations significantly influence the robustness and convergence of IGA models. While stable solutions were obtained in most nonlinear scenarios, challenges related to contact modelling, damage evolution, and locking phenomena require careful parameter selection.

Despite these advantages, several limitations remain, including the current maturity of the IGA implementation in LS-DYNA, which affects robustness under parallel execution and stability for coarse discretisations. Additional challenges were observed in preprocessing workflows and modelling of highly nonlinear damage behaviour, indicating areas for further development before full industrial deployment.

Overall, this study demonstrates that IGA is a viable and effective approach for nonlinear crash analysis, capable of accurately predicting both material and structural behaviour under complex loading conditions. While strong agreement with experimental and FE results was achieved across all validation levels, further improvements in solver capabilities, contact formulations, and CAD-integrated workflows are required for fully converged large-scale simulations.

Nevertheless, the IGA framework shows strong potential as a next-generation simulation method for crashworthiness applications, offering a technologically advanced alternative to conventional finite element approaches.

7

Future Work

Several key areas for future development are identified to improve the robustness, efficiency and industrial applicability of the IGA framework.

7.1 Solver Development and Robustness

A primary focus for future work should be the continued development of IGA implementations within industrial finite element solvers such as LS-DYNA. In particular, improvements in solver robustness, numerical stability, and parallel scalability are essential. Enhanced user control over nonlinear solution strategies is also required to support complex analyses involving large deformations, contact interactions, and progressive damage evolution.

Moreover, the development of advanced stabilisation techniques and improved handling of spline-based discretisations would significantly enhance numerical reliability. These improvements are particularly critical for solid formulations operating under crash-relevant loading conditions.

7.2 Preprocessing and CAD Integration

Another critical research direction is the development of robust and automated preprocessing workflows. Current limitations in tools such as ANSA highlight the need for improved support of IGA-specific features, including spline generation, patch definition, and trimming operations.

Future work should aim to achieve a seamless CAD-to-analysis integration, enabling direct utilisation of design geometries without extensive manual intervention. Such developments would reduce model preparation time, minimise user dependency, and improve consistency between geometric design and simulation models.

7.3 Numerical Formulation and Continuity Effects

From a numerical perspective, further studies are needed to better understand the influence of spline continuity on nonlinear solution behaviour. While higher-order continuity improves accuracy and smoothness, it also introduces additional coupling, which can affect stability and computational performance.

Adaptive modelling strategies that balance numerical accuracy and efficiency should be explored. These may include selective refinement techniques or hybrid approaches that combine IGA with conventional finite elements to optimise performance in critical regions.

7.4 Verification, Validation, and Debugging Tools

The development of dedicated verification and debugging tools for IGA models is essential for industrial adoption. In particular, improved diagnostics for knot vector validity, patch continuity, and geometry-to-analysis mapping consistency would significantly enhance model reliability and reduce preprocessing effort.

In addition, further work is required on experimental validation and the development of robust error estimation techniques, which are critical for establishing confidence in IGA predictions and ensuring reliable performance across different applications.

7.5 Extension to Large-Scale Industrial Applications

Finally, future developments should focus on extending IGA capabilities to full-scale industrial crash simulations, including integration into full-vehicle crash models, the development of efficient shell formulations for thin-walled structures, and the improvement of contact algorithms for spline-based discretisations. These advancements are necessary to enable scalable, efficient, and reliable large-scale simulations, thereby supporting the broader industrial adoption of IGA in automotive crashworthiness applications.

Bibliography

[1] Xiwei Li and Dongdong Wang. On the significance of basis interpolation for accurate lumped mass isogeometric formulation. *Computer Methods in Applied Mechanics and Engineering*, 402:115623, 2022. DOI: 10.1016/j.cma.2022.115533.

[2] Encyclopedia of continuum mechanics. 2020. DOI: 10.1007/978-3-662-55771-6.

[3] Thomas J. R. Hughes, John A. Cottrell, and Yuri Bazilevs. Isogeometric analysis: CAD, finite elements, NURBS, exact geometry and mesh refinement. *Computer Methods in Applied Mechanics and Engineering*, 194(39–41):4135–4195, 2005. DOI: 10.1016/j.cma.2004.10.008.

[4] J. Austin Cottrell, Thomas J. R. Hughes, and Yuri Bazilevs. *Isogeometric Analysis: Toward Integration of CAD and FEA*. John Wiley & Sons, 2009. DOI: 10.1002/9780470749081.

[5] Gra.zyna Mr'owka-Nowotnik and Jan Sieniawski. Influence of heat treatment on the microstructure and mechanical properties of 6005 and 6082 aluminium alloys. *Journal of Materials Processing Technology*, 162–163:367–372, 2005. DOI: 10.1016/j.jmatprotec.2005.02.115.

[6] Yuri Bazilevs, Victor M. Calo, J. Austin Cottrell, John A. Evans, Thomas J. R. Hughes, Stuart Lipton, Michael A. Scott, and Thomas W. Sederberg. Isogeometric analysis using T-splines. *Computer Methods in Applied Mechanics and Engineering*, 199(5–8):229–263, 2010. DOI: 10.1016/j.cma.2009.02.036.

[7] V. P. Nguyen, C. Anitescu, S. P. A. Bordas, and T. Rabczuk. Isogeometric analysis: An overview and computer implementation aspects. *Mathematics and Computers in Simulation*, 117:89–116, 2015. DOI: 10.1016/j.matcom.2015.05.008.

[8] P. Wriggers. *Nonlinear Finite Element Methods*. Springer, 2 edition, 2016. DOI: 10.1007/978-3-540-71001-1.

[9] T. J. R. Hughes. *The Finite Element Method: Linear Static and Dynamic Finite Element Analysis*. Prentice-Hall, 1987. DOI: 10.1016/0045-7825(87)90013-2.

[10] H. Casquero and M. Golestanian. Vanquishing volumetric locking in quadratic NURBS-based discretizations of nearly-incompressible linear elasticity: CAS elements. *Computational Mechanics*, 73:1241–1252, 2024. DOI: 10.1007/s00466-023-02409-5.

[11] L. Piegl and W. Tiller. *The NURBS Book*. Springer-Verlag, 2 edition, 1997. DOI: 10.1007/978-3-642-59223-2.

[12] S. Hartmann, D. Benson, L. De Lorenzis, et al. Current status of LS-DYNA isogeometric analysis in crash simulation. In *14th International LS-DYNA Users Conference*, Detroit, Michigan, USA, 2016. LSTC.

[13] Michael J. Borden, Michael A. Scott, John A. Evans, and Thomas J. R. Hughes. Isogeometric finite element data structures based on Bézier extraction of NURBS. *International Journal for Numerical Methods in Engineering*, 87(1–5):15–47, 2011. DOI: 10.1002/nme.2968.

[14] Yury Novozhilov and Lukas F. Leidinger. Trimmed IGA solids in LS-DYNA: CADFEM findings – interpolation mesh with material, background mesh for calculations. In *EMEA Ansys Transportation Summit and International LS-DYNA Conference*, Munich, Germany, 2025.

[15] O. C. Zienkiewicz, R. L. Taylor, and J. Z. Zhu. *The Finite Element Method: Its Basis and Fundamentals*. Elsevier, 6 edition, 2005. DOI: 10.1016/C2009-0-24909-9.

[16] Livermore Software Technology Corporation (LSTC). *LS-DYNA Theory Manual*, 2025. LS-DYNA R16.

[17] Yuri Bazilevs, Victor M. Calo, Thomas J. R. Hughes, and Yongjie Zhang. Isogeometric fluid–structure interaction: theory, algorithms, and computations. *Computational Mechanics*, 43(1):3–37, 2008. DOI: 10.1007/s00466-008-0315-x.

[18] David J. Benson, Yuri Bazilevs, Ming-Chen Hsu, and Thomas J.R. Hughes. Isogeometric shell analysis: The reissner–mindlin shell. *Computer Methods in Applied Mechanics and Engineering*, 199(5–8):276–289, 2010. DOI: 10.1016/j.cma.2009.05.011.

[19] G. Charca Ramos, M. Stout, R. E. Bolmaro, J. W. Signorelli, and P. Turner. Study of a drawing-quality sheet steel. i: Stress/strain behaviors and lankford coefficients by experiments and micromechanical simulations. *International Journal of Solids and Structures*, 47(17):2285–2293, 2010. DOI: 10.1016/j.ijsolstr.2010.04.023.

[20] A. L. Gurson. Continuum theory of ductile rupture by void nucleation and growth. *Journal of Engineering Materials and Technology*, 99:2–15, 1977. DOI: 10.1115/1.3443401.

[21] Y. Bai and T. Wierzbicki. A new model of metal plasticity and fracture with pressure and Lode dependence. *International Journal of Plasticity*, 24:1071–1096, 2008. DOI: 10.1016/j.ijplas.2007.09.004.

[22] P.W. Bridgman. *Studies in Large Plastic Flow and Fracture with Special Emphasis on the Effects of Hydrostatic Pressure*. Metallurgy and metallurgical engineering series. McGraw-Hill, 1952.

[23] G. R. Johnson and W. H. Cook. Fracture characteristics of three metals subjected to various strains, strain rates and temperatures. *Journal of Engineering Materials and Technology*, 107:31–48, 1985. DOI: 10.1016/0013-7944(85)90052-9.

[24] M. G. Cockcroft and D. J. Latham. Ductility and the workability of metals. *Journal of the Institute of Metals*, 96:33–39, 1968.

[25] Oweis Al-Karawi and Victor Mathiesen. Verification of plane stress material model behaviour in solid 3d-structures. Master's thesis, Chalmers University of Technology, Gothenburg, Sweden, 2024. Conducted in collaboration with Volvo Cars Corporation.

[26] F. Neukamm, M. Feucht, and A. Haufe. Considering damage history in crashworthiness simulations. In *Proceedings of the 7th European LS-DYNA Conference*, 2009.

[27] Qi Zhang, Xiaochang Xu, and Yu Wang. Effect of Mg/Si ratio on the bendability and anisotropic bend behavior of extruded 6000-series Al alloy. *Materials*, 16(9):3599, 2023. DOI: 10.3390/ma16093599.

[28] Marco Negozio, Antonio Segatori, Riccardo Pelaccia, Barbara Reggiani, Sara Di Donato, and Lorenzo Donati. Modeling of recrystallization behaviour of AA6xxx aluminum alloy during extrusion process. *Transactions of Nonferrous Metals Society of China*, 34(10):3170–3184, 2024. DOI: 10.1016/S1003-6326(24)66600-8.

[29] Li-Wen Xue, Hai-Long Jia, Pin-kui Ma, Jia-Wang Song, Min Zha, and Hui-Yuan Wang. Influence of Mg and Cu on precipitation behaviors and mechanical properties of Al–Si alloys. *Materials Science and Engineering: A*, 908:146775, 2024. DOI: 10.1016/j.msea.2024.146775.

[30] Endre Hennum, Knut Marthinsen, and Ulf H. Tundal. Effect of microstructure on the precipitation of β-mg$_2$si during cooling after homogenisation of Al–Mg–Si alloys. *Metals*, 14(2):215, 2024. DOI: 10.3390/met14020215.

[31] Carl Enstedt and Shivani Shivani. Correlating mechanical testing and simulations: A study on lateral crushing of aluminum extrusions. Master's thesis, Linköping University, Linköping, Sweden, 2025. Conducted in collaboration with Volvo Cars Corporation.

[32] Lars Lodgaard and Nils Ryum. Precipitation of dispersoids containing Mn and/or Cr in Al–Mg–Si alloys. *Materials Science and Engineering A*, 283(1–2):144–152, 2000. DOI: 10.1016/S0921-5093(00)00734-6.

[33] Nazlin Bayat, Tomas Carlberg, and Miroslav Cieslar. In-situ study of phase transformations during homogenization of 6005 and 6082 Al alloys. *Journal of Alloys and Compounds*, 725:504–509, 2017. DOI: 10.1016/j.jallcom.2017.07.149.

[34] A. Debih and E. Ouakdi. Anisotropic thermomechanical behavior of aa6082 aluminum alloy. *International Journal of Materials Research*, 109(1):34–41, 2018. DOI:10.3139/146.111580.

A

Appendix 1: Shell, Solid and IGA model results comparison

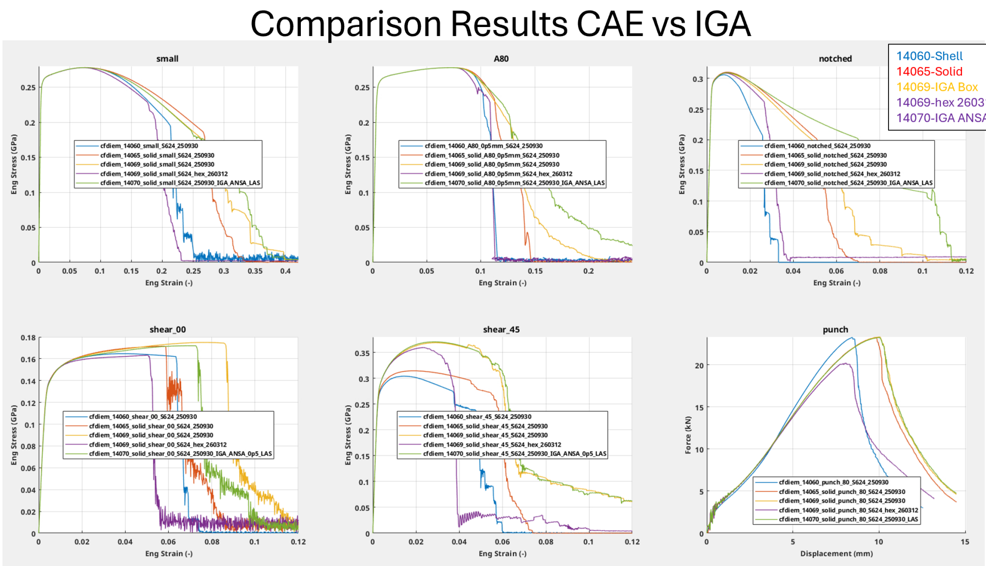

Figure A.1: Comparison of FEA and IGA results for six coupon tests using shell, solid, IGA Box, IGA ANSA, and mapped solid (hexahedral) material models

B

Appendix 2: Additional Materials results

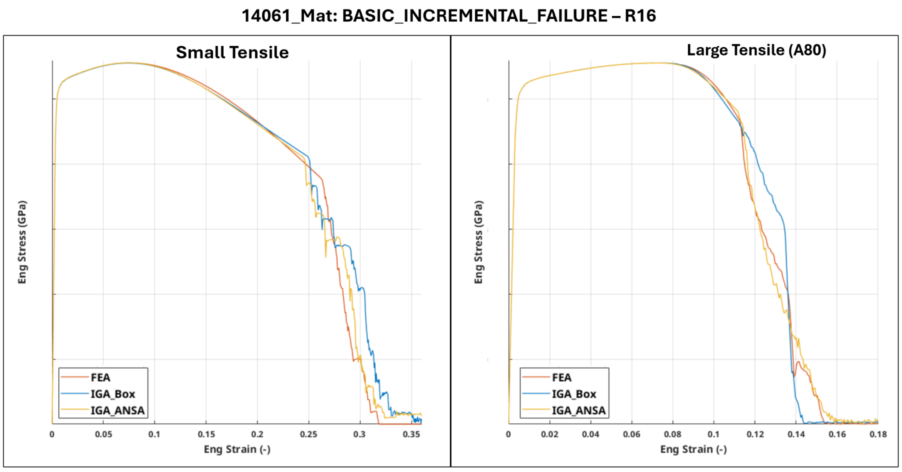

Figure B.1: Comparison of FEA and IGA stress–strain responses for tensile and large tensile (A80) tests with the BASIC_INCREMENTAL_FAILURE damage model

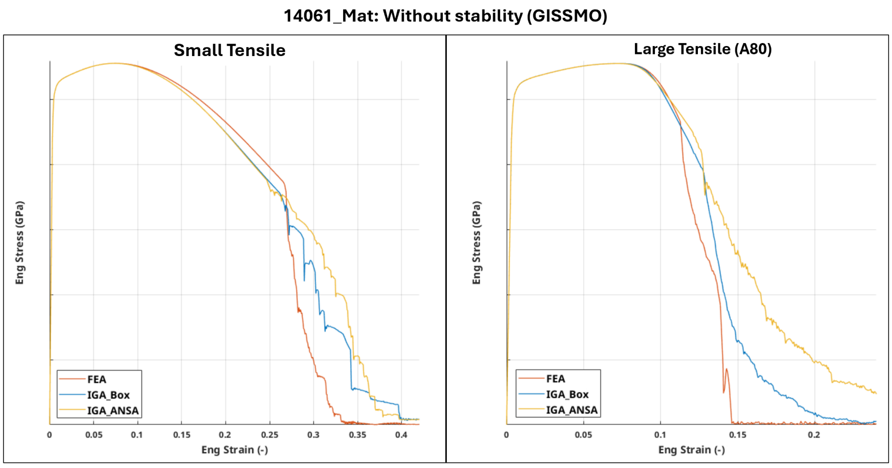

Figure B.2: Comparison of FEA and IGA stress–strain responses for tensile and large tensile (A80) coupon without GISSMO damage model

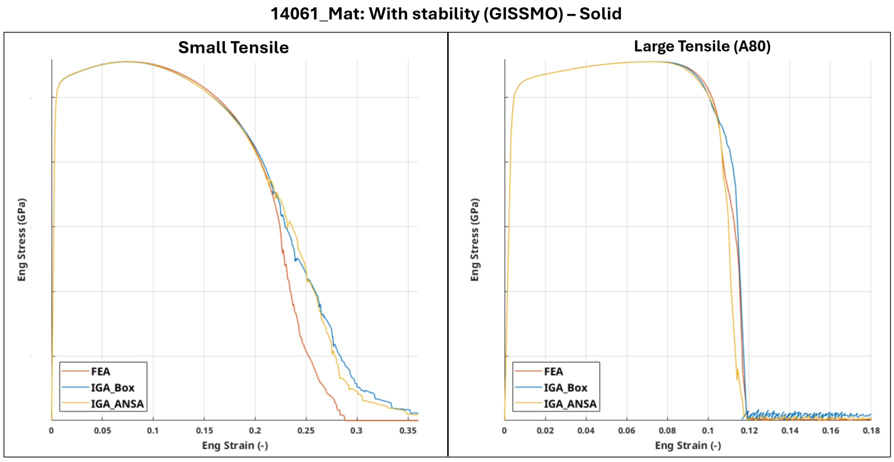

Figure B.3: Comparison of FEA and IGA stress–strain responses for tensile and large tensile (A80) coupon with GISSMO damage model

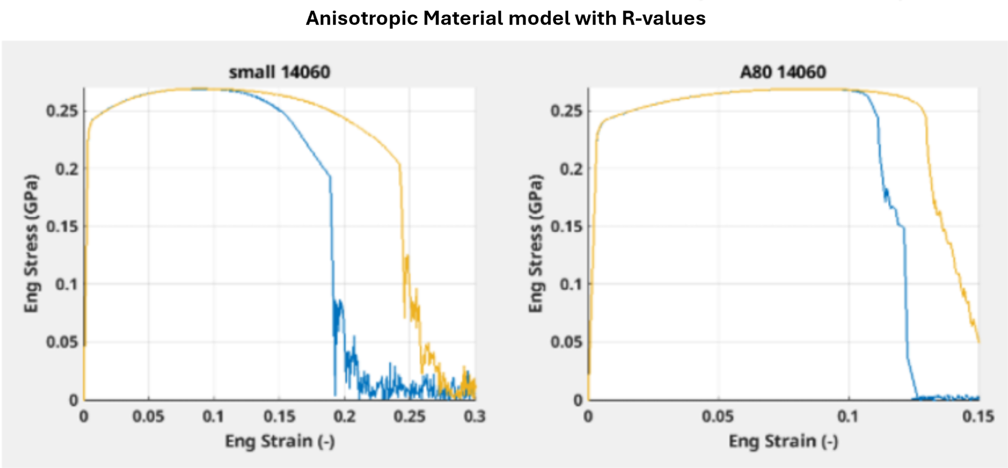

Figure B.4: IGA predictions of anisotropic material behaviour using an implemented anisotropic (R-Value) constitutive model, with improved agreement to experimental results when R-values are included in the CAE model for the 0° (Blue) and 90° directions (Yellow).

C

Appendix 3: Comparative Stress Contour Results of IGA and FEA

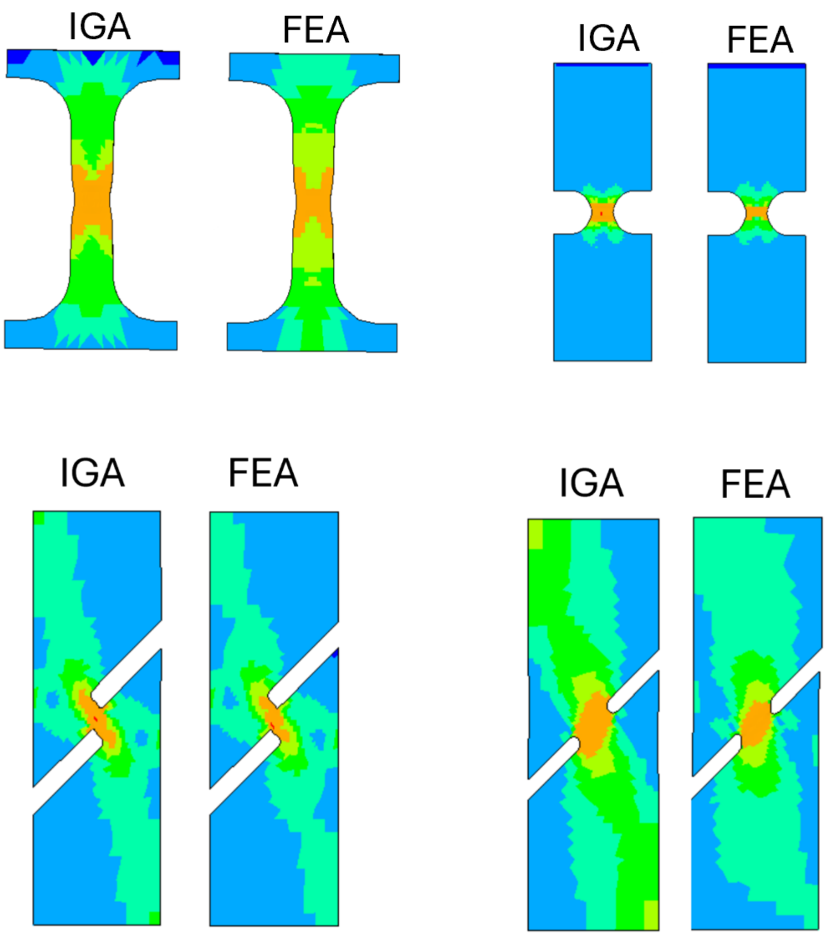

Figure C.1: Comparison of stress contour distributions between conventional FEA and IGA for representative coupon specimens, demonstrating good overall correlation across all investigated samples.

DEPARTMENT OF INDUSTRIAL AND MATERIAL SCIENCE
CHALMERS UNIVERSITY OF TECHNOLOGY
Gothenburg, Sweden
www.chalmers.se

CHALMERS
UNIVERSITY OF TECHNOLOGY